AD 728108

HDL-TR-1650

ANALYSIS OF M125 [illegible]

by

J. L. Overton

June 1971

U.S. ARMY MATERIEL COMMAND

HARRY DIAMOND LABORATORIES

WASHINGTON, D.C. 20438

DISCLAIMER NOTICE

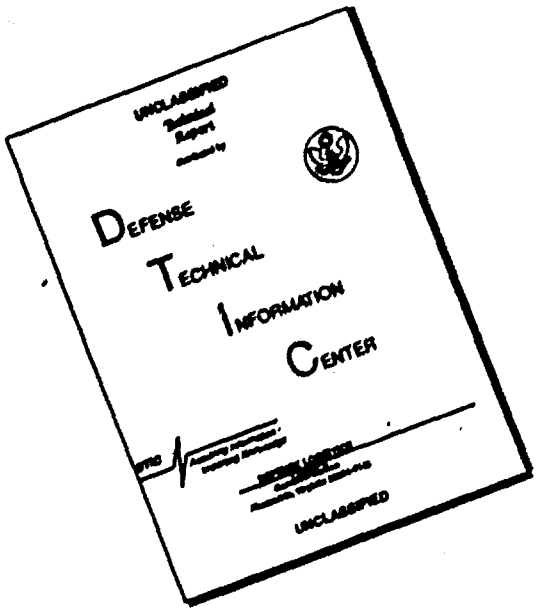

THIS DOCUMENT IS BEST QUALITY AVAILABLE. THE COPY FURNISHED TO DTIC CONTAINED A SIGNIFICANT NUMBER OF PAGES WHICH DO NOT REPRODUCE LEGIBLY.

14. KEY WORDS	LINK A		LINK B		LINK C	
	ROLE	WT	ROLE	WT	ROLE	WT
safety and arming devices	8	3				
proximity fuze	8	3				
turns-to-arm	8	3				
escapements	8	3				
artillery fuzes	8	3				

ABSTRACT (cont'd.)

with experimental data and with each other. Comparison of the analytic and experimental results indicates that the model should take into account a slight increase in damping torque with increasing speed. One possibility for modifying the model to include this effect is discussed. A final topic of the analysis is a treatment of the turns-to-arm characteristic as it actually applies to various artillery weapons.

The findings in this report are not to be construed as an official Department of the Army position unless so designated by other authorized documents.

Citation of manufacturers' or trade names does not constitute an official indorsement or approval of the use thereof.

Destroy this report when it is no longer needed. Do not return it to the originator.

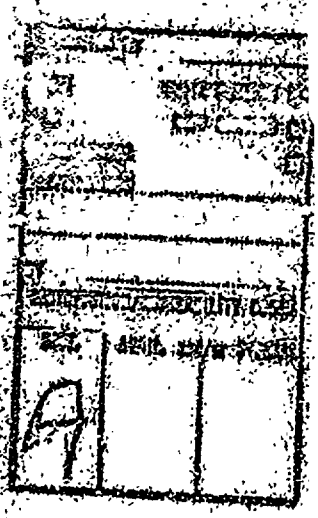

Unclassified
Security Classification

DOCUMENT CONTROL DATA - R & D

(Security classification of title, body of abstract and indexing annotation must be entered when the overall report is classified)

1. ORIGINATING ACTIVITY (Corporate author) Harry Diamond Laboratories Washington, D.C. 20438	2a. REPORT SECURITY CLASSIFICATION Unclassified 2b. GROUP

3. REPORT TITLE

ANALYSIS OF M125 BOOSTER MECHANISM

4. DESCRIPTIVE NOTES (Type of report and inclusive dates)

5. AUTHOR(S) (First name, middle initial, last name)

David L. Overman

6. REPORT DATE	7a. TOTAL NO. OF PAGES	7b. NO. OF REFS
June 1971	68	4

8a. CONTRACT OR GRANT NO.	9a. ORIGINATOR'S REPORT NUMBER(S)
b. PROJECT NO. HDL Proj: 72742	HDL-TR-1550
c. AMCMS Code: 4810.16.47341.01	9b. OTHER REPORT NO(S) (Any other numbers that may be assigned this report)
d. DA: none	

10. DISTRIBUTION STATEMENT

Approved for public release; distribution unlimited.

11. SUPPLEMENTARY NOTES	12. SPONSORING MILITARY ACTIVITY
	USAMC

13. ABSTRACT

A mathematical analysis of the M125 booster safety and arming mechanism is presented. It provides a better insight into the mode of operation of the M125 and the effect of certain design parameter variations on the mechanism's performance. This analysis was made in support of product improvement efforts on the S&A device for the M514A1E1 artillery proximity fuze.

Equations of motion involving 33 design and operating parameters of the mechanism and both phases of the rotor's movement are developed and discussed. In developing an expression for the damping torque due to escapement action, it is assumed that the rotor's angular velocity is proportional to the square root of the driving torque. Computations for the damping coefficient are based on a prior detailed dynamic analysis of the escape wheel and pallet covering their six phases of motion per cycle. The final equations of motion are nonlinear; digital simulation methods were therefore used for their solution. Illustrated and discussed are time, rate, and turns-to-arm versus spin speed; also, displacement, velocity, and acceleration are considered as a function of time at high- and low-spin rates (100 and 30 rps).

By making certain simplifying assumptions, the equations were reduced and solved analytically. Turns-to-arm results for the detailed and simplified mathematical models are compared (cont'd. on reverse)

DD FORM 1 NOV 68 1473 REPLACES DD FORM 1473, 1 JAN 64, WHICH IS OBSOLETE FOR ARMY USE.

Unclassified
Security Classification

AD

DA: none
AMCMS Code: 4810.16.47341.01
HDL Proj: 72742

HDL-TR-1550

ANALYSIS OF M125 BOOSTER MECHANISM

by
David L. Overman

June 1971

U.S. ARMY MATERIEL COMMAND
HARRY DIAMOND LABORATORIES
WASHINGTON, D.C. 20438

A B S T R A C T

A mathematical analysis of the M125 booster safety and arming mechanism is presented. It provides a better insight into the mode of operation of the M125 and the effect of certain design parameter variations on the mechanism's performance. This analysis was made in support of product improvement efforts on the S&A device for the M514A1E1 artillery proximity fuze.

Equations of motion involving 33 design and operating parameters of the mechanism and both phases of the rotor's movement are developed and discussed. In developing an expression for the damping torque due to escapement action, it is assumed that the rotor's angular velocity is proportional to the square root of the driving torque. Computations for the damping coefficient are based on a prior detailed dynamic analysis of the escape wheel and pallet covering their six phases of motion per cycle. The final equations of motion are nonlinear; digital simulation methods were therefore used for their solution. Illustrated and discussed are time, rate, and turns-to-arm versus spin speed; also, displacement, velocity, and acceleration are considered as a function of time at high- and low-spin rates (100 and 30 rps).

By making certain simplifying assumptions, the equations were reduced and solved analytically. Turns-to-arm results for the detailed and simplified mathematical models are compared with experimental data and with each other. Comparison of the analytic and experimental results indicates that the model should take into account a slight increase in damping torque with increasing speed. One possibility for modifying the model to include this effect is discussed. A final topic of the analysis is a treatment of the turns-to-arm characteristic as it actually applies to various artillery weapons.

CONTENTS

FIGURES

CONTENTS (cont'd.)

FIGURES

1. INTRODUCTION

The work described in this report was conducted in CY69 as part of the effort directed toward a product improved safety and arming (S&A) device for the M514A1E1 artillery proximity fuze. To provide delayed mechanical arming for this fuze, a modification of the M125 booster mechanism (fig. 1) was to be used. The M125 provides safety during storage, transportation, handling, and firing of several current artillery munitions. This safety is achieved primarily by sensing the force generated by projectile spin. Two spring-biased rotor locks are unlatched, and an unbalanced rotary explosive train interrupter is driven into alignment with the primary explosive initiator in the fuze. Motion of the rotor is retarded by a gear train and runaway escapement that generates a damping force roughly proportional to the square of the rotor's velocity. This arrangement delays alignment of the explosive train until the projectile has traveled a fixed distance from the gun muzzle. The safe separation distance is essentially constant for all muzzle velocities for a given weapon and, as discussed in section 4 of this report, can be expressed by the number of projectile revolutions or "turns-to-arm" required for arming the device.

The analysis described in this report was initiated to gain a better insight into the operation of the M125 booster-type mechanism and to show how certain design parameters influence its operation. An objective was to obtain an equation that would predict the performance of the device and that could be used to evaluate the effects of variations in such parameters as inertia, mass, and center of gravity of the rotor. Although 33 different design parameters of the mechanism are included in the analysis, the method of incorporating these variables is usually greatly simplified when compared with the real situation. For example, torque loss at the gear meshes is introduced as a simple value for the average mesh efficiency, and escapement action is treated by calculating an average damping coefficient.

2. MATHEMATICAL ANALYSIS

2.1 General Equation

Behavior of the S&A device (fig. 2) can be described by the following equation relating the rotor driving torque (τ) and the torques that resist rotor motion (neglecting forces due to Coriolis accelerations).

$$I_R\ddot{\theta} + R = \tau \qquad (1)$$

The equation is straightforward except for the R term, which is a function of practically every geometric, dynamic, material, and friction property of the mechanism. These include the pallet and gear weights and inertias, pivot sizes and location, friction coefficients, gear-mesh efficiencies, and geometric and impact loss properties of the escapement.

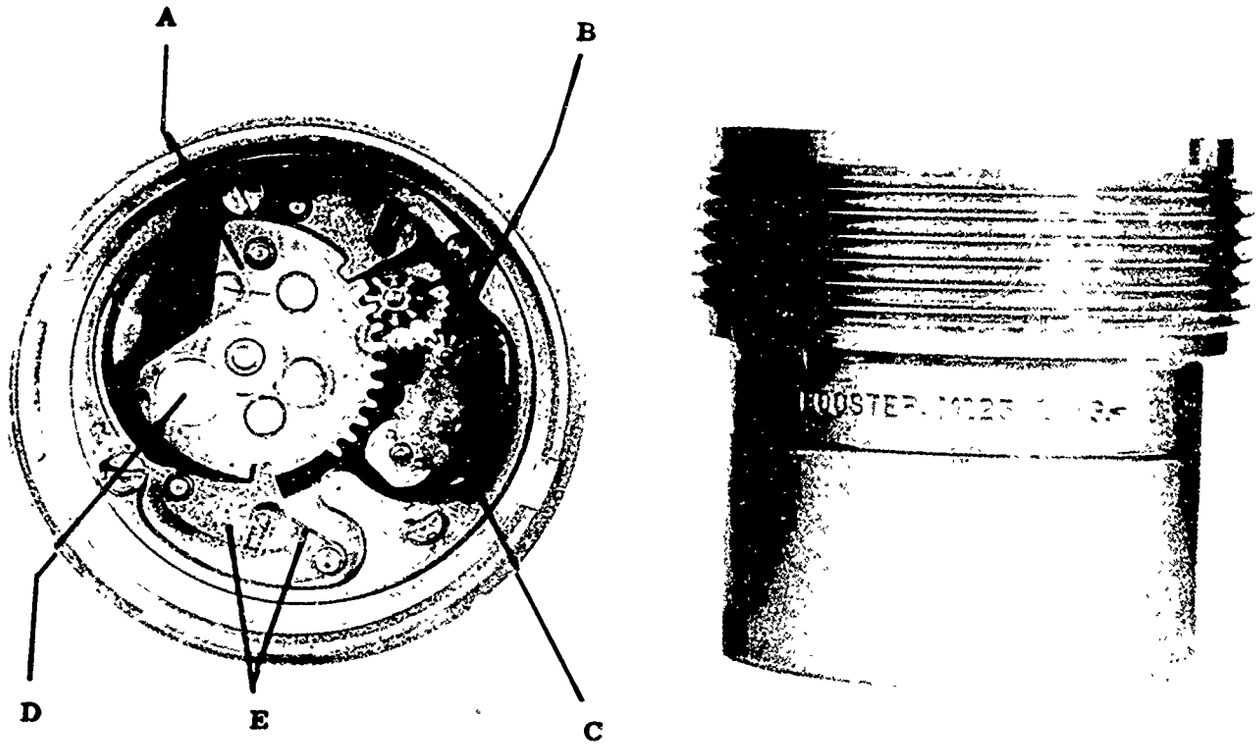

A. Rotor
B. Gear Train
C. Escapement
D. Detonator M17 (Unarmed Position)
E. Detent and Spring

Figure 1. Photograph of booster mechanism (M125A1) with lucite movement plate

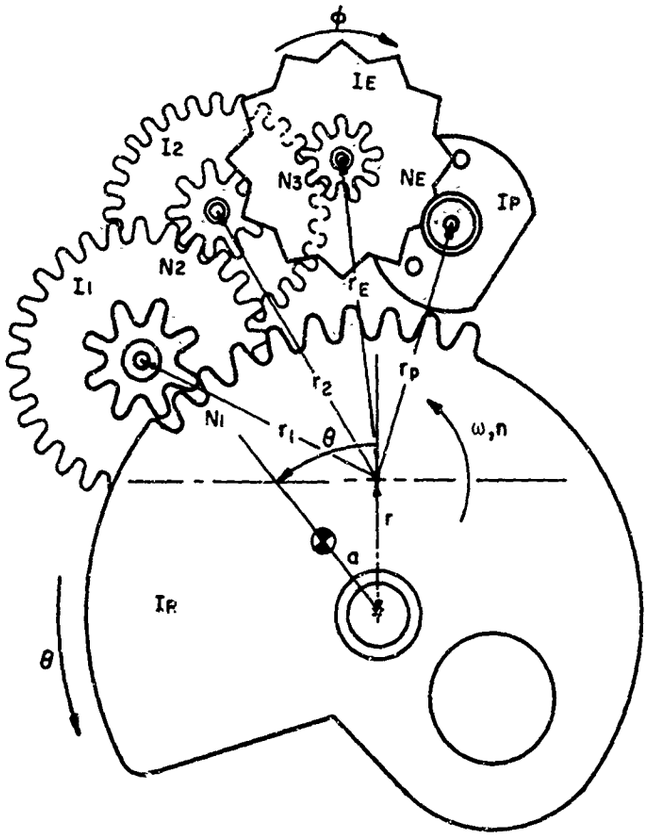

Figure 2. Nomenclature used in the analysis

The resisting torque term (R) is broken down into the following three separate terms.

$$R=R_I + R_F + R_E \tag{2}$$

where

R_I = inertial resistance of the gear train and escape wheel,
R_F = frictional resistance of the gear train and escapement, and
R_E = resistance due to escapement action.

Motion of the rotor actually occurs in two phases. The first phase has the rotor coupled to the gear train and escapement; the second phase is after the rotor disengages from the gear train and swings free before impacting its stop. Equation 1, with different initial conditions, applies to both phases, but the term (R) will include only the rotor pivot friction torque during the second phase.

2.2 Rotor Drive Torque

Referring to figure 3, the rotor-drive torque (τ) is obtained as follows:

$$\tau = F\, a \sin(\pi - B) \tag{3}$$

$$F = m_R X \omega^2 ; \tag{4}$$

from the law of sines,

$$\sin(\pi - B) = \sin B = (r/X)\sin\theta ; \tag{5}$$

substituting equations (4) and (5) into equation (3),

$$\tau = a r m_R \omega^2 \sin\theta . \tag{6}$$

2.3 Inertial Resistance

Making use of the fact that inertias are reflected as the square of the linkage ratio between the components, R_I is given simply as

$$R_I = \left[N_1^2 I_1 + (N_1 N_2)^2 I_2 + (N_1 N_2 N_3)^2 I_E \right] \ddot{\theta} . \tag{7}$$

2.4 Frictional Resistance

The term for frictional resistance is obtained by summing the effective pivot friction torques and taking into account an average efficiency of torque transmission for each gear mesh and the escapement mesh. Thus,

$$R_F = \mu\omega^2 \left[m_R r r_{pR} + \frac{N_1}{\eta_1} m_1 r_1 r_{p_1} + \frac{N_1 N_2}{\eta_1 \eta_2} m_2 r_2 r_{p_2} + \frac{N_1 N_2 N_3}{\eta_1 \eta_2 \eta_3} m_E r_E r_{pE} \right.$$

$$\left. + \frac{N_1 N_2 N_3 P N_E}{\eta_1 \eta_2 \eta_3 \eta_E} m_p r_p r_{pp} \right] + \tau(1 - \eta_1 \eta_2 \eta_3 \eta_E) + \tau_0 \tag{8}$$

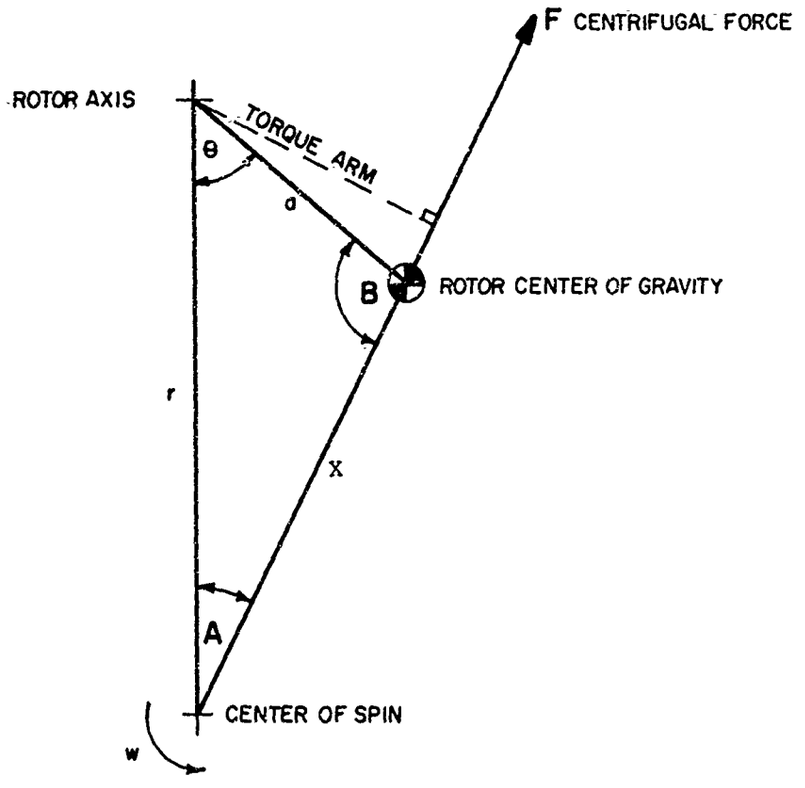

Figure 3. Geometry used to determine rotor drive torque

where

(a) The first term is due to friction at the pivots.

(b) The rotor mass is assumed to be concentrated at the rotor pivot.

(c) The second term is due to losses at each mesh.

(d) The mesh efficiencies η_1, η_2, and η_3 are assumed independent of load.

(e) The coefficient of friction (μ) is assumed constant throughout the mechanism.

(f) The nominal effective linkage ratio (PN_E) and efficiency (η_E) for the escapement are assumed constant. The linkage ratio is the same as the ratio of the angular velocity of the pallet to the angular velocity of the escape wheel when they are engaged. The factor (P) represents the assumed fraction of time that the pallet pins are engaged with the escape wheel. The value of η_E would be an estimate of the average effect of friction on energy loss during escapement action.

(g) The starting torque (t_ϕ) represents the minimum spin speed at which the mechanism (less rotor locks) begins to function (see eq 29).

2.5 Resistance Due To Escapement Action

The term R_E is much more difficult to evaluate than are the R_I and R_F terms. In theory, R_E is proportional to the square of the mean escape-wheel velocity ($\dot{\bar{\phi}}$), although an exponent of slightly more or less than 2 may best represent the behavior of the actual mechanism. Assuming velocity squared resistance,

$$R_E' = C_E \dot{\bar{\phi}}^2 \tag{9}$$

where R_E' is the resistance torque at the escape-wheel and C_E is a "damping coefficient" at the escape-wheel, which is a function of the pallet inertia, effective escape-wheel inertia, coefficients of restitution and friction during interaction of the pallet pins with the escape-wheel tooth, and the detailed geometry of the parts and of their interaction.

Escapement resistance as seen at the rotor is

$$R_E = \frac{N_1 N_2 N_3}{\eta_1 \eta_2 \eta_3} R_E' , \tag{10}$$

but

$$\dot{\bar{\phi}} = N_1 N_2 N_3 \dot{\theta} . \tag{11}$$

Substituting equations (9) and (11) into equation (10),

$$R_E = \frac{C_E (N_1 N_2 N_3)^3 \dot{\theta}^2}{\eta_1 \eta_2 \eta_3} . \tag{12}$$

Thus, $$R_E = C\dot{\theta}^2 \quad , \tag{13}$$

where $$C = C_E \frac{(N_1 N_2 N_3)^3}{\eta_1 \eta_2 \eta_3} \quad . \tag{14}$$

The major problem is to obtain a reasonable theoretical estimate for the value of the coefficient C_E. Use will be made of some theoretical work that was done on a verge-type runaway escapement by Arthur Hausner of HDL and the Virginia Military Institute (VMI), Department of Physics,[1] Based on the following simplifying assumptions,

(a) Instantaneous, inelastic collisions,

(b) Constant value of the linkage ratio (N_E),

(c) No recoil of the escape wheel,

(d) Linkage ratio being the same for both entrance and exit pallet pin action,

and the equations of motion developed by VMI, Hausner derived the following expressions for the average escape-wheel velocity ($\bar{\dot{\phi}}$) for a constant torque (τ_E) applied to the escape wheel. Thus, for:

NO-FREE MOTION (continuous engagement between pallet and escape wheel),

$$\bar{\dot{\phi}}_{NFM} = \sqrt{\frac{\tau_E \psi}{I_p N_E^2}} \left(\sqrt{\frac{I_e}{2\,(I_e + N_E^2 I_p)}} \right); \tag{15}$$

ALL-FREE MOTION (engagement between pallet and escape wheel only during impact),

$$\bar{\dot{\phi}}_{AFM} = \sqrt{\frac{\tau_E \psi}{I p N_E^2}} \left(\sqrt{\frac{I_e + N_E^2 I p}{2 I_e}} \right); \tag{16}$$

HALF-FREE MOTION and HALF-ENGAGED MOTION,

$$\bar{\dot{\phi}}_{.IH} = \sqrt{\frac{\tau_E \psi}{I_p N_E^2}} \left(\sqrt{\frac{I_e}{I_e + N_E^2 I_p}} + \sqrt{\frac{I_e + N_E^2 I_p}{I_e}} \right); \tag{17}$$

where, by reflecting inertias by the square of the gear ratios,

$$I_e = I_E + \frac{I_3}{N_3^2 (N_3 N_2)^2} + \frac{I_1}{(N_3 N_2 N_1)^2} + \frac{I_R}{} \tag{18}$$

[1] "A Study of The Dynamics Of An Untuned Clock Mechanism," VMI Dept. of Physics, Lexington Virginia; under contract CST-1224 (DAI-49-186-ORD (P)-100) with Harry Diamond Labs, 1 Sept 1953.

and ψ is the angle subtended by half an escape-wheel tooth.

Letting $$I' = I_e + N_E^2 I_p \tag{19}$$

and solving each expression for $\tau_E/\ddot{\phi}^2$, the corresponding values for damping coefficient (C_E) from equation (9) are as follows when recognizing that $\tau_E = R'_E$.

$$C_{NFM} = \frac{2N_E^2 I_p I'}{\psi I_e} , \tag{20}$$

$$C_{AFM} = \frac{2N_E^2 I_p I_e}{\psi I'} , \tag{21}$$

and

$$C_{HH} = \frac{N_E^2 I_p (I'+I_e)^2}{2\psi\, I' I_e} . \tag{22}$$

Although these are fairly simple equations used to describe the relatively complex action of the escapement components, it should be remembered that they result from a detailed dynamic analysis of the escapement that included the variable linkage ratios for camming at the pallets and the separation of one cycle of motion into six different phases.

Examination of equations (20), (21), and (22) reveals that they can all be combined into a single equation as follows:

$$C_E = \frac{2N_E^2 I_p [PI' + (1-P) I_e]^2}{\psi \qquad I' I_e} , \tag{23}$$

where P is the fraction of engaged motion so that

P=0 for AFM,
P=0.5 for HH, and
P=1 for NFM.

Equation (23) can be further reduced, and equation (19), used to obtain an equation for the damping coefficient at the escape wheel in terms of the variables P and N_E. Thus,

$$C_E = \frac{2N_E^2 I_p (I_e + PN_E^2 I_p)^2}{\psi\, I_e (I_e + N_E^2 I_p)} . \tag{24}$$

It is now necessary to examine the relationship between P and N_E. Possible values of the linkage ratio for the M125A1 booster escapement were obtained from measurements made on a 50-to-1 scale layout using basic dimensions. (This linkage ratio problem is treated analytically for zero diameter

pallet pins by Minnix.[1]) The graphical procedure is illustrated in figure 4 for position 3 of the entrance pallet pin, and the results are shown in figure 5. Note the following with respect to figure 5.

(a) The linkage ratio for this escapement is not constant.

(b) The variation in linkage ratio is different for the entrance and exit pallet pins.

(c) The tip surface of the escape-wheel tooth (rather than the impulse face) comes into contact with the pallet-pin surface somewhere between positions 5 and 6. (This neglects dynamic considerations.)

(d) Each position on the abscissa corresponds to 4 deg of motion of the pallet (not the escape-wheel).

(e) The curve labeled "average" (and more specifically the straight line fit of the curve) will be used to represent the linkage ratio characteristics for the escapement.

(f) Because the linkage ratio is poorly defined after position 5 and the tips of the teeth are normally rounded instead of pointed as assumed in the graphical analysis, the linkage ratio curve will be considered to end at position 5 for the purposes of this analysis.

The linkage ratio is meaningful only when there is engaged motion of the escapement, that is, when the impulse face of an escape-wheel tooth is engaged with a pallet pin. Thus, for fully engaged motion, the pallet pin starts at the root of this impulse face and moves in engagement to the tip of the impulse face. The average linkage ratio during this excursion would be about halfway between the extreme values of $N_R = 1.05$ and $N_T = 1.98$; or, $N_{E_1} = 1.515$. For the case of all-free motion ($P = 0$), the pallet pin barely contacts the tip of the impulse face, so that the average linkage ratio is the value of N_T; or, $N_{E_0} = 1.98$. For the case of half-free motion and half-engaged motion, the pallet pin is assumed to contact the impulse face about halfway along its length and then to move in engagement upward to the tip. The average linkage ratio during this excursion would be a value halfway between the midpoint value of 1.515 and the tip value of 1.98; or, $N_{E_{.5}} = 1.747$. The relationship between N_E and P, which expresses these linkage ratios, is

$$N_E = N_T - \left(\frac{N_T - N_R}{2}\right) P. \qquad (25)$$

Solutions to this equation can be read from figure 5 by using the auxillary abscissa labeled "P" and the

[1] "The Development of a Mathematical Model of the Detached Lever Escapement," by Dr. Richard B. Minnix, VMI Physics Dept. under contract no. DA-49-186-AMC-176 (D) with Harry Diamond Laboratories, July 1968.

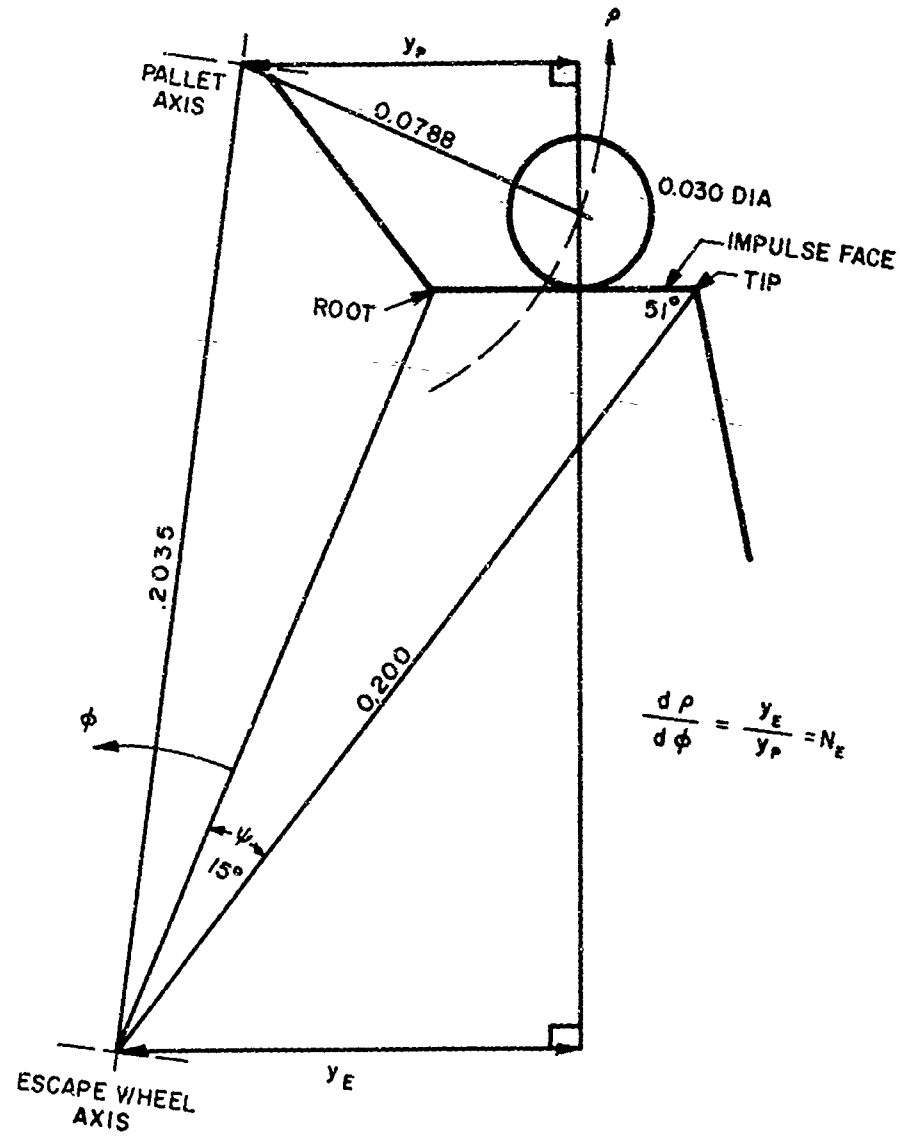

Figure 4. Graphical procedure used to determine escapement linkage ratios

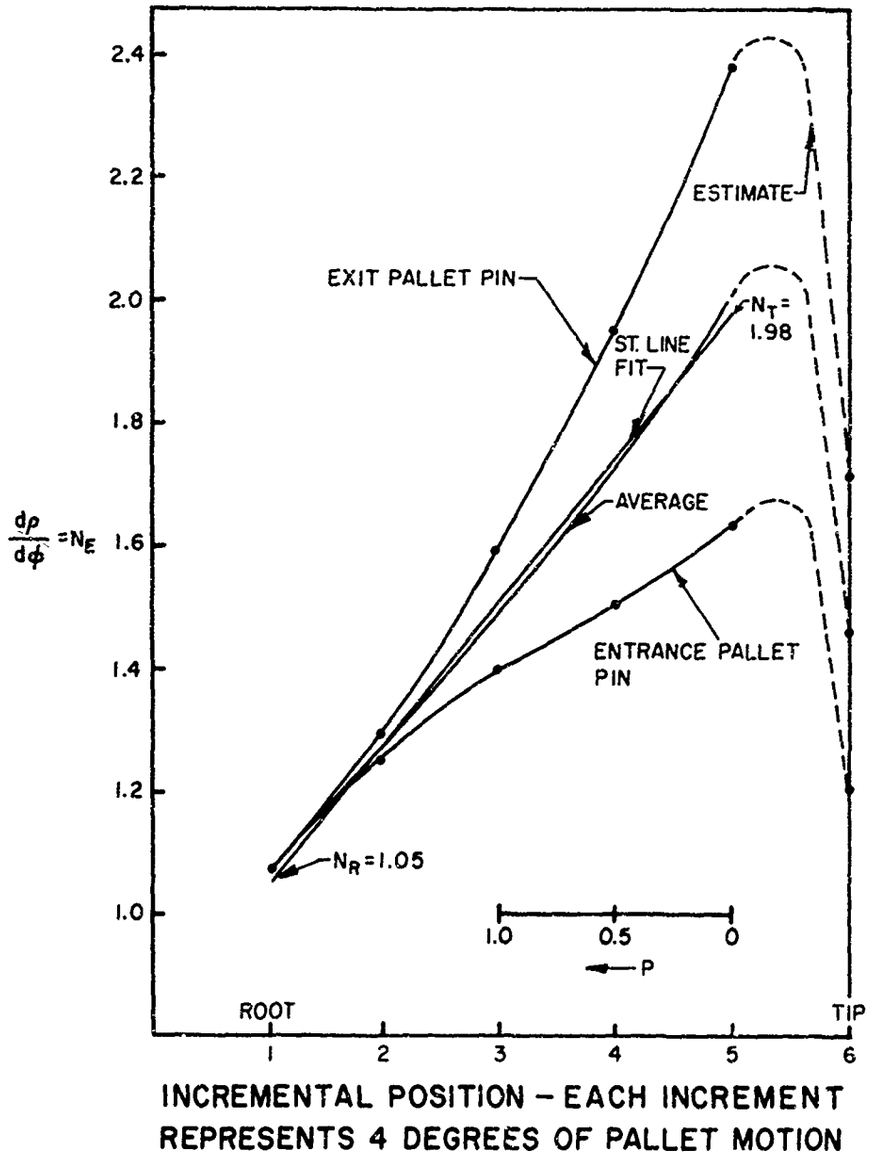

Figure 5. Graph of escapement linkage ratios

straight line fit to the average linkage ratio curve. For example, choosing a value of 25 percent engaged motion, the corresponding value of N_E is 1.86. Equation (25) could be substituted into equation (24) to obtain an expression for the escapement damping coefficient in terms of the single variable P; this is not done here, because the resulting equation would be cumbersome. Instead, the results will be plotted in section 3.4, and this new curve will be used to choose a theoretical damping coefficient for the analysis.

2.6 Final Equations of Motion

The final equation for the coupled phase of the motion is obtained by substituting equations (2), (6), (7), (8), and (13) into equation (1).

The result is

$$I_{Re}\ddot{\theta} + C\dot{\theta}^2 = (arm_R\eta^4 \sin\theta - \mu f)\omega^2 - \tau_0 , \qquad (26)$$

where the following additional substitutions have been made.

The effective rotor inertia I_{RE} is

$$I_{Re} = I_R + \frac{R_I}{\ddot{\theta}} . \qquad (27)$$

It is assumed that

$$\eta_1 = \eta_2 = \eta_3 = \eta_4 = \eta , \qquad (28)$$

and (f) equals the bracketed term in equation (8).

The equation for the value of τ_0 representing the threshold of motion is simply

$$\tau_0 = \omega_0^2 (arm_R\eta^4 \sin\theta_0 - \mu f). \qquad (29)$$

Note that inclusion of the term τ_0 makes the final equation of motion valid only for the conditions of $\omega > \omega_0$.

The equation of motion for phase 2, where the rotor has uncoupled from the gear train, is obtained from equation (26) by eliminating the nonapplicable terms. Thus,

$$I_R\ddot{\theta} = m_R r\omega^2 (a \sin\theta^{\lambda} - \mu r_{pR}), \qquad (30)$$

where the initial conditions on θ and $\dot{\theta}$ for phase 2 are the final values of θ and $\dot{\theta}$ from phase 1, and the phase 2 motion covers an excursion of 45 deg.

3. EVALUATION OF TERMS

The numerical values used for the various mechanism parameters in the following calculations represent one set of measurements made on a particular group of booster devices (see acknowledgements). Thus, they should only be considered as approximations (accurate to within 2 or 3 percent) of the actual values that would result from other measurements made

on other devices of the same design.

3.1 Rotor Drive Torque

Upon substitution of the values for a, r, and m_R, the rotor drive torque from equation (6) becomes

$$\tau = 0.0941 \times 0.225 \times (19.58/386.4) \times 2.54 \times 4\pi^2 n^2 \sin\theta = 0.1075 n^2 \sin\theta \text{ gm-cm}, \quad (31)$$

where (n) is the spin rate in revolutions per second. During engagement with the gear train, the rotor center of gravity makes an excursion of 80 deg, starting at $\theta_0 = 37$ deg. As an example of the range of driving torques under which this device is called upon to operate, the torque at θ_0 for a spin speed of 3000 rpm is 162 gm-cm. At 25,000 rpm, the initial driving torque becomes 11,230 gm-cm, and the maximum torque when $\theta = 90$ deg is 18,690 gm-cm. This is a range of roughly 115 to 1.

The average driving torque ($\bar{\tau}$) during the first phase of the motion is obtained by using the mean value (c) for sin θ between 37 and 117 deg in equation (31), which gives

$$c = \frac{57.3}{80} \int_{37^0}^{117^0} \sin\theta \, d\theta = 0.8972 \quad (32)$$

Thus,

$$\bar{\tau} = 0.0964 \, n^2 \text{ gm-cm} \quad (33)$$

for phase one.

3.2 Equivalent Rotor Inertia

Evaluation of equations (27) and (7) to obtain the effective rotor inertia yields

$$I_{Re} = 12200 \times 10^{-6} + (5.25)^2 (130 \times 10^{-6}) + (5.25 \times 3)^2 (31 \times 10^{-6}) + (5.25 \times 3 \times 3)^2 (27 \times 10^{-6}) \quad (34)$$

$$= 10^{-6}[12200 + 3583 + 7690 + 60280],$$

or

$$I_{Re} = 0.08375 \text{ gm-cm-sec}^2$$

Note that I_{Re} is approximately seven times as large as I_R alone, and that the effect of the very small escape-wheel inertia when reflected as the square of its gear ratio [$(N_1 N_2 N_3)^2 = 2233$] accounts for about 72 percent of the total effective rotor inertia.

3.3 Friction Torque

Substituting values into the first or pivot friction term of equation (8) and denoting the bracketed part of this term by the symbol (f) yields

$$\mu_3 f = \frac{(2\pi)^2 (2.54)^2 \mu n^2}{g} \left[19 \times 0.225 \times 0.0050 + \frac{5.25}{\eta_1} \times 1.18 \times 0.436 \times 0.0248 + \frac{5.25 \times 3}{\eta_1 \eta_2} \times 0.50 \times 0.505 \times 0.0181 + \frac{5.25 \times 3 \times 3}{\eta_1 \eta_2 \eta_3} \times 0.43 \times 0.520 \times 0.0165 + \frac{5.25 \times 3 \times 3 \times 0.25 \times 1.86}{\eta_1 \eta_2 \eta_3 \eta_E} \times 0.62 \times 0.433 \times 0.0165 \right], \quad (35)$$

where n is the spin speed in revolutions per second and the value of 1.86 for the average linkage ratio of the escapement corresponds to 25 percent engaged motion (see fig. 5). Section 3.4 presents more on the selection of P = 0.25.

From equation (35) with the help of equation (28), f becomes (including the conversion factor of $4\pi^2$)

$$f = 0.260 \left(0.278 + \frac{0.067}{\eta} + \frac{0.072}{\eta^2} + \frac{0.174}{\eta^3} + \frac{0.0973}{\eta^4}\right),$$

or

$$f = 0.0723 + \frac{0.0174}{\eta} + \frac{0.0187}{\eta^2} + \frac{0.0452}{\eta^3} + \frac{0.0253}{\eta^4} \text{ gm-cm-sec}^2, \quad (36)$$

and

$$f = 0.1790 \text{gm-cm-sec}^2 \text{ when } \eta \text{ equals unity.}$$

The last two terms in equation (8) will be evaluated in section 3.5 as they appear in equation (26).

3.4 Escapement Damping

To obtain a value for damping due to escapement action, a value for the effective escape-wheel inertia (I_e) is needed. Substituting values into equation (18) yields

$$I_e = \left\{27 + \frac{31}{3^2} + \frac{130}{(3 \times 3)^2} + \frac{12200}{(3 \times 3 \times 5.25)^2}\right\} \times 10^{-6} \quad (37)$$

$$= [27 + 3.444 + 1.605 + 5.465] \times 10^{-6}$$

$$= 37.514 \times 10^{-6} \text{gm-cm-sec}^2.$$

Note that the gear train and rotor contribute an effective increase in escape-wheel inertia of only about 10.5/27 = 39 percent.

From equation (25) with the values of N_T and N_R from figure 5,

$$N_E = 1.980 - 0.465P. \qquad (38)$$

Using equation (38) and the value of I_e from equation (37) in equation (24), the values of escapement damping coefficient (C_E) versus percent engaged motion (P) can be computed. These results are shown on figure 6.

On the basis of rough calculations, a value of P=0.25 or 25 percent engaged motion for the escapement is selected as a trial value that should give results in the neighborhood of experimental results. (More on the selection of P in sections 5 and 8 of the report.) This makes $C_E = 520 \times 10^{-6}$ gm-cm-sec^2 and $N_E = 1.86$, as used in equation (35). With this value for C_E and using condition (28), the escapement damping from equation (13) becomes

$$R_E = 520 \times 10^{-6} \ (5.25 \times 3 \times 3)^3 \frac{\dot{\theta}^2}{\eta^3}, \qquad (39)$$

or

$$R_E = \frac{54.85}{\eta^3} \ \dot{\theta}^2,$$

and from equation (14),

$$C = \frac{54.85}{\eta^3} \text{ gm-cm-sec}^2 . \qquad (40)$$

These calculations of the escapement damping coefficient dramatically illustrate how minute changes in the geometry of interaction for the escapement (such as escape-wheel diameter, pallet pin locations, and center distance), can produce very large deviations in arming time for the mechanism. The major variable in the equation for C_E is the nominal linkage ratio (N_E) or the corresponding percentage of engaged motion (P) for the escapement, and N_E (which always appears squared) is strictly a function of these geometric parameters as shown by figure 4. (The pallet inertia is also a major factor in the value of C_E, but it is far less sensitive to tolerance variations than is N_E.) Slight changes in the actual geometry of interaction would be expected to produce large changes in the effective value of N_E and thereby large change in C_E. However, C_E is a very small value which is subsequently multiplied by a very large constant--the cube of the overall gear ratio--to produce the effective damping of the rotor motion. Therefore, relatively small changes in geometry should produce relatively large variations in the overall damping coefficient (C), which in turn is a major determinant of arming time for a given rotor drive torque as demonstrated in equation (59), section 6.

3.5 Final Equations With Coefficients

Inserting the numerical values from equations (31), (34), and (40) into the final equations of motion (26) and (30) yields

For Phase I

$$0.08375 \ \ddot{\theta} + \frac{54.95}{\eta^3} \dot{\theta}^2 = n^2 \ [0.1075 \ \eta^4 \sin \theta - \mu f] - \tau_0 , \qquad (41)$$

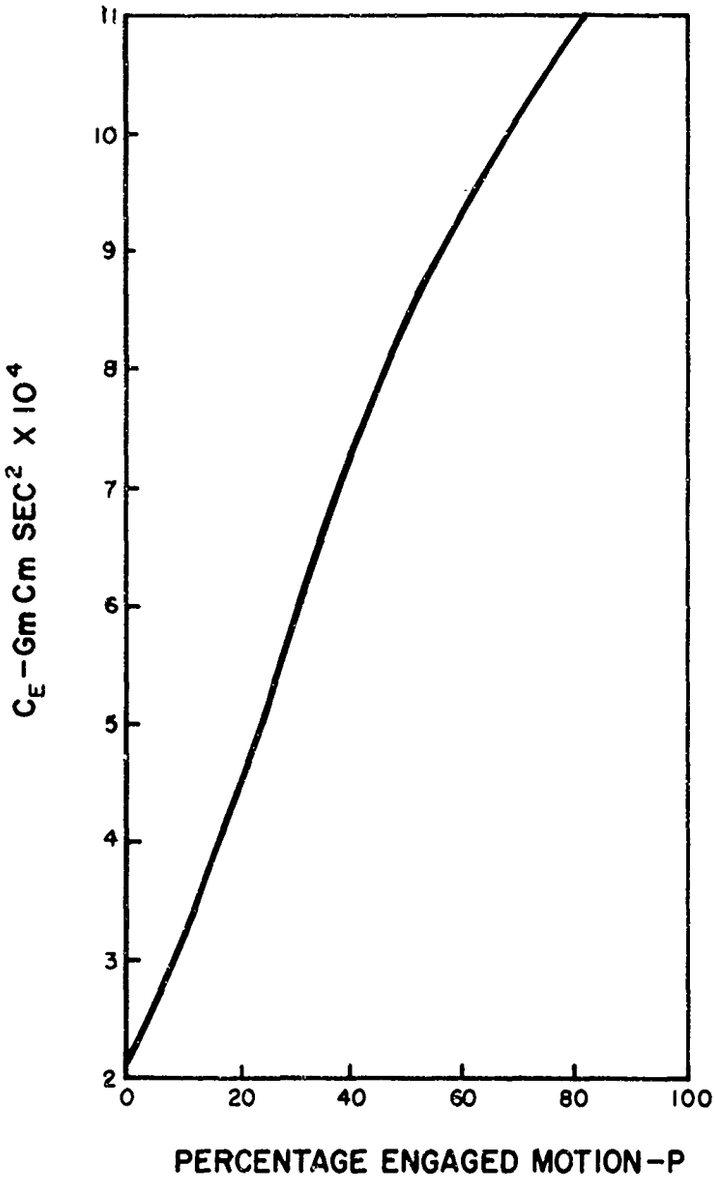

Figure 6. Escapement damping coefficient versus percentage of engaged motion

where the spin rate (n) is in revolutions per second and equation (36) defines the value for (f).

Combining equations (29) and (31),

$$\tau_0 = n_0^2 (0.1075 \eta^4 \sin \theta_o - \mu f). \qquad (42)$$

For Phase II (from equation 30)

$$0.0122 \ddot{\theta} = n^2 (0.1075 \sin \theta - 0.0723 \mu), \qquad (43)$$

where the values for θ extend from 117 to 162 deg.

In these equations, η and μ are left in as variables so a good fit can be obtained between theory and experiment. Note also that n_0 and the numerical coefficient (54.85) of the $\dot{\theta}^2$ term are also to be considered as variables in the fitting process. A first estimate for μ and η can be obtained by examining table I, which shows the coefficients for the bracketed term in equation (41) for $\theta = \theta_o = 37$ deg and various values of η. The value (μmax) is the coefficient of friction for which there would be no net rotor starting torque.

From this table, values of $\eta = 0.98$ and $\mu = 0.15$ are selected for use in the initial computations with the expectation that they may require revision to obtain better agreement between theory and experiment. With a value of $\eta = 0.98$, the equation of motion for phase 1 becomes:

$$0.08375 \ddot{\theta} + 58.28 \dot{\theta} = n^2 (0.0991 \sin \theta - 0.1850 \mu) - \tau_0 \qquad (44)$$

where

$$\tau_0 = n_0^2 (0.0597 - 0.1850 \mu) \text{ gm-cm} \qquad (45)$$

Table I. Values for the bracketed term of equation (41) with θ = 37 deg

η	[0.0647 n^4 - μf]	μmax
1.00	0.0647 - 0.1790 μ	0.361
0.99	0.0621 - 0.1819 μ	0.342
0.98	0.0597 - 0.1850 μ	0.322
0.97	0.0573 - 0.1882 μ	0.304
0.96	0.0549 - 0.1916 μ	0.287
0.95	0.0527 - 0.1952 μ	0.270
0.94	0.0505 - 0.1988 μ	0.254
0.93	0.0484 - 0.2027 μ	0.239
0.92	0.0463 - 0.2067 μ	0.224
0.91	0.0444 - 0.2109 μ	0.210
0.90	0.0424 - 0.2153 μ	0.197
0.85	0.0338 - 0.2408 μ	0.140
0.80	0.0265 - 0.2734 μ	0.097

4. TURNS-TO-ARM CHARACTERISTIC

As mentioned in section 1, the M125 booster-type mechanism integrates the spin force and arms after a constant number of turns of the projectile. This produces a theoretically constant arming distance independent of muzzle velocity or spin speed. This characteristic can be visualized simply as follows. The relationship between muzzle velocity (V) and spin speed (n) for an artillery weapon is

$$V = nBT, \tag{46}$$

where B is the bore diameter (in feet per caliber) and T is the inverse "twist" of the rifling at the muzzle (in calibers per revolution or turn). Assuming air drag is negligible, the projectile will reach a distance (d) from the muzzle in a time (t_a) of

$$t_a = \frac{d}{V} = \frac{d}{nBT} . \tag{47}$$

For a runaway escapement timer mechanism, arming time (t_a) is inversely proportional to the square root of the driving torque τ; or,

$$t_a \propto \sqrt{\frac{1}{\tau}} . \tag{48}$$

For a centrifugally driven device, average torque is proportional to the square of the spin speed; or,

$$\tau \propto n^2 . \tag{49}$$

Using equation (49) in (48), the arming time for the M125 booster-type mechanism is basically inversely proportional to the spin speed; or

$$t_a = \frac{N}{n} , \tag{50}$$

where N is a proportionality constant. Substituting equation (50) in equation (47), the arming distance is seen to be

$$d = NBT, \tag{51}$$

which is a constant value independent of spin speed or muzzle velocity. The value of N is the turns-to-arm for the device, and the product BT is the feet traveled per turn of the projectile for a given weapon. Table II gives values of BT for various artillery weapons, and figure 7 shows the theoretical arming distance versus turns-to-arm for these weapons.

The nominal value of N is the basic performance characteristic for each particular mechanism design. For this reason, turns-to-arm is used to compare and describe different designs, and it is used as a quality control parameter for production. Typical turns-to-arm values are represented by four of the Army's booster device designs as follows. (These are nominal values probably accurate to within ±2 turns.)

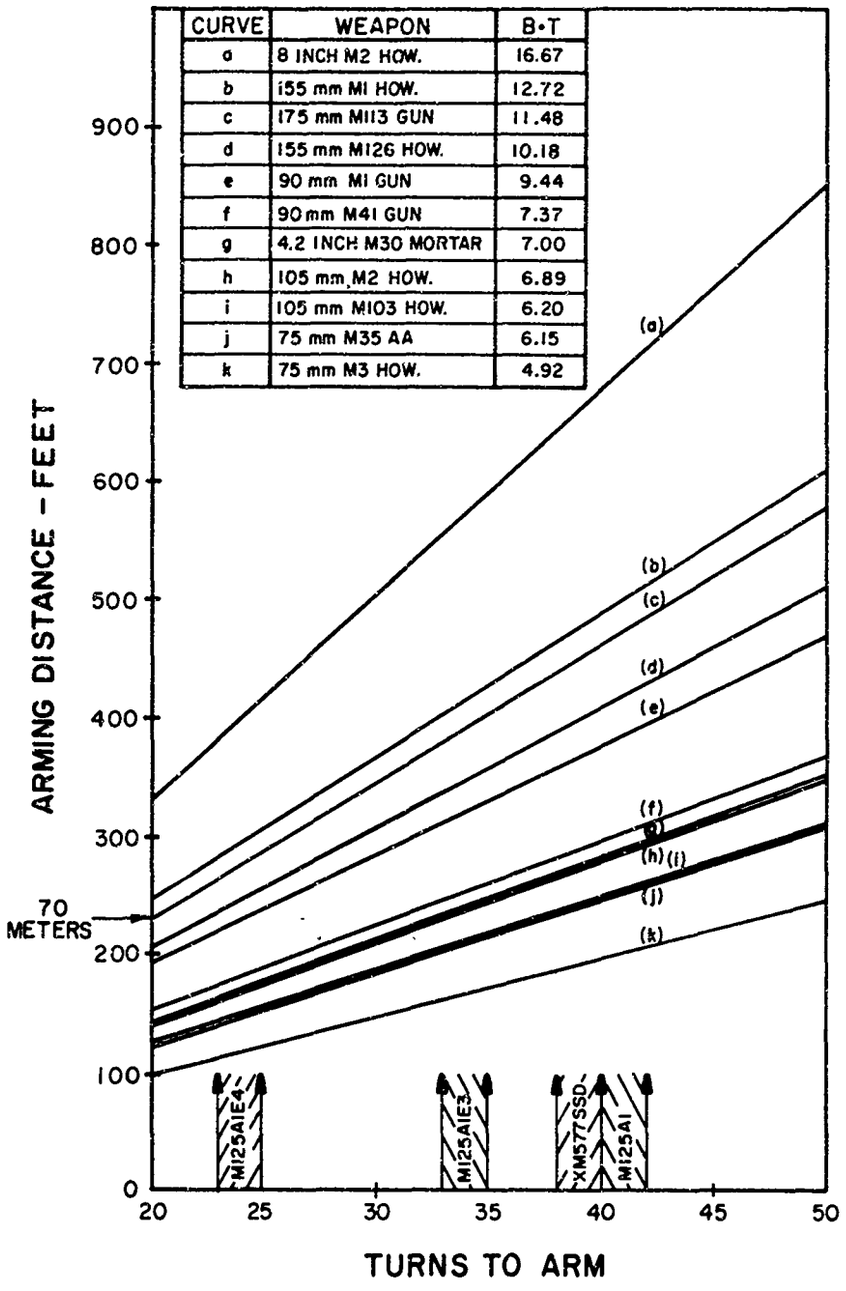

Figure 7. Arming distance versus turns-to-arm for various weapons

Table II. Characteristics of various artillery weapons

Caliber	Weapon	Twist	Bore-ft	BT - ft/turn
75 mm	M3 Howitzer	20	0.246	4.92
75 mm	M35 AA	25	0.246	6.15
90 mm	M1 Gun	32	0.295	9.44
90 mm	M41 Gun	25	0.295	7.37
105 mm	M103 Howitzer	18	0.345	6.20
105 mm	M2 Howitzer	20	0.345	6.89
4.2 in.	M30 Mortar	20	0.350	7.00
155 mm	M126 Howitzer	20	0.509	10.18
155 mm	M1 Howitzer	25	0.509	12.72
175 mm	M113 Gun	20	0.574	11.48
8 in.	M2 Howitzer	25	0.667	16.67

Booster designs	No. of turns-to-arm
M125A1	41
M125A1E3	34
M125A1E4	24
Safe Separation Device (SSD) for XM577	39

In general, the larger turns-to-arm values represent a slower running mechanism.

Many field-test results have verified that the arming distance for the M125-type device is essentially constant for all zones or charges of firings from a particular weapon. However, discrepancies and dispersions about the predicted mean performance do occur and these may be attributed to:

(a) Variations in friction and manufacturing tolerances from unit to unit.

(b) The fact that the threshold spin friction (the τ_0 term in equation 8) influences performance at low spin as demonstrated in the next three sections of this report.

(c) The fact that the arming cycle does not necessarily begin at the muzzle. (The actual starting point for the arming cycle depends on where the spin-drive forces overcome the setback-induced friction forces tending to prevent motion of the moving parts.)

(d) The fact that, in some cases, there may be slip between the projectile and barrel at the muzzle such that the effective twist is different than the theoretical twist.

(e) Variations in air drag at the different velocities, projectile surface finishes, and ambient air conditions.

5. EXPERIMENTAL DATA

The arming time of ten M125A1 booster units was measured at various spin speeds by using a high-speed Kodak horizontal, belt-driven spinner having slip rings. Start-and-stop signals for an electronic timer (accurate to 1 μsec) were obtained by breaking contact to ground as one of the detents was released manually after achieving the desired speed, and making contact to ground as the rotor hit an insulated stop contact upon reaching the fully armed position. Each unit was run once at each spin speed, starting at the lowest speed and going to the highest. Thus, there may have been some "wearing-in" of the mechanisms as the tests progressed.

The results obtained from these experiments are plotted in three different ways on figures 8, 9, and 10. The curves are plotted through the average value obtained for all 10 units while the vertical bars with tick marks represent the extremes of the data obtained. Figure 8 is a plot of time versus spin speed and is generally hyperbolic in shape (see eq 50). Figure 9 shows inverse arming time or arming cycle rate (number of potential armings per second) versus spin speed and is approximately a straight line as expected (invert eq 50). Figure 10 (curve a) is a plot of turns-to-arm (nt_a) versus spin speed with a highly magnified scale for the ordinate. Note on figures 9 and 10 that the result is not the ideal straight line and that the curves are essentially smooth. The curious curvature in these results was a major motivation for the theoretical analysis covered by this report. If the same unusual tendency to relative increase in turns-to-arm at the higher spin speeds could be predicted theoretically, not only would the experimental data be verified but the mathematical model would be automatically validated. Unfortunately, as shown in sections 6 and 7, the present model does not predict the upward curvature at higher spin speeds, so that either the model is not fully accurate (although still highly useful) or the experimental data contained some systematic error which is a function of spin speed or test method.

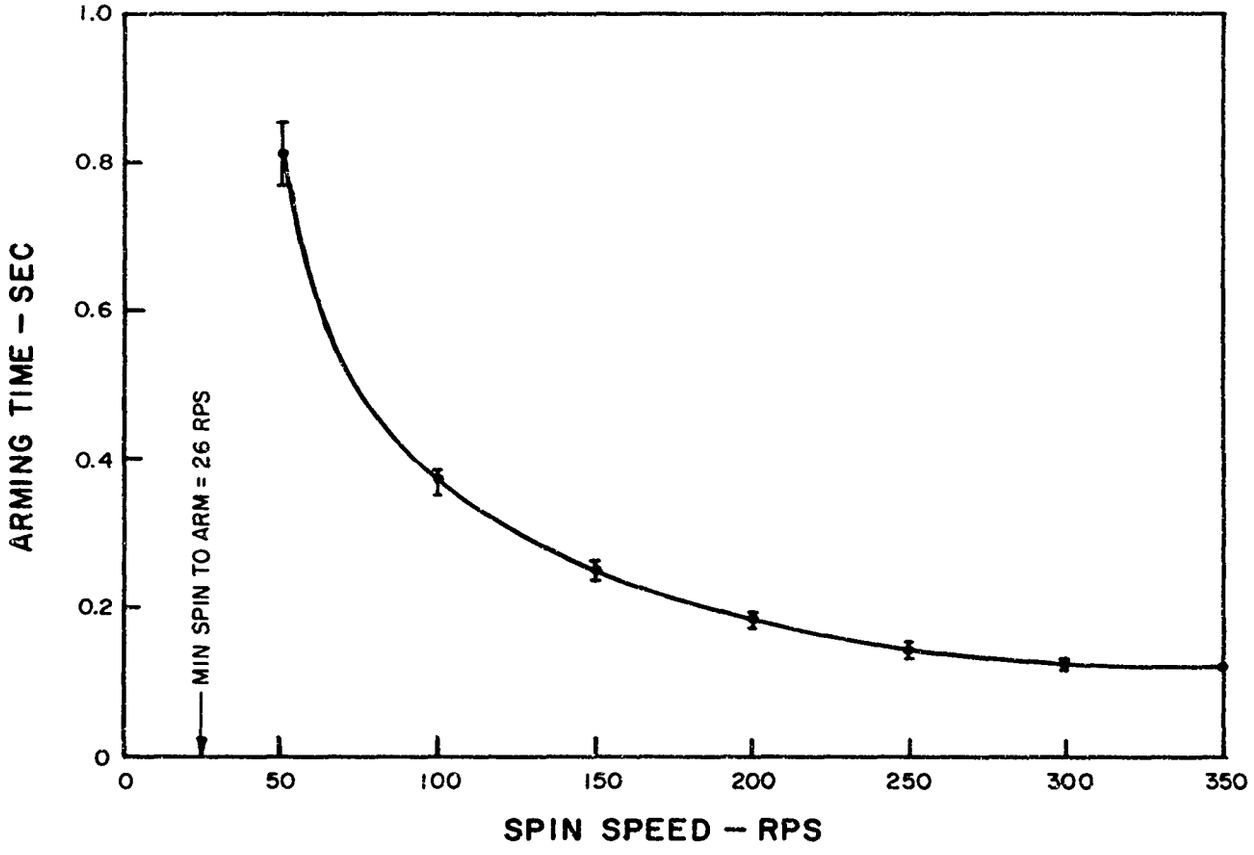

Figure 8. Experimental arming time versus spin-speed results

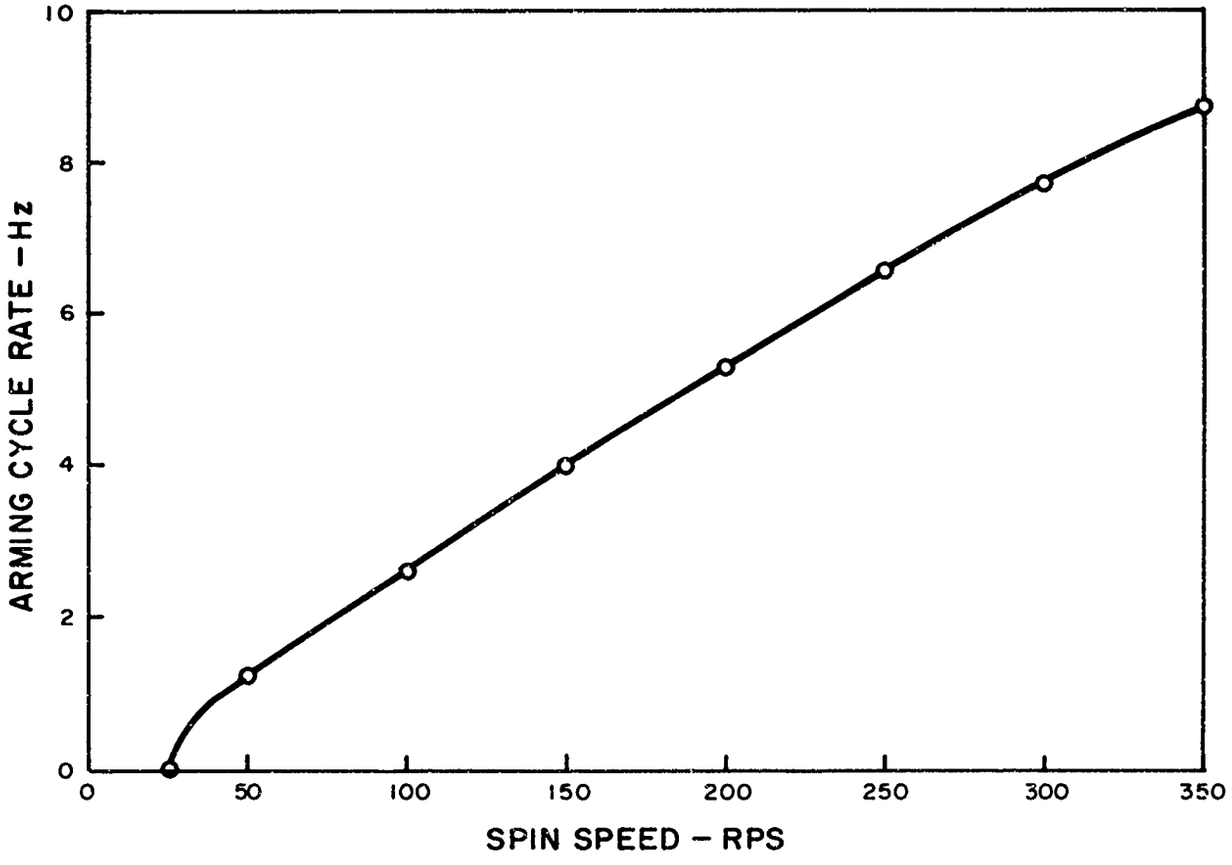

Figure 9. Experimental arming cycle rate versus spin speed

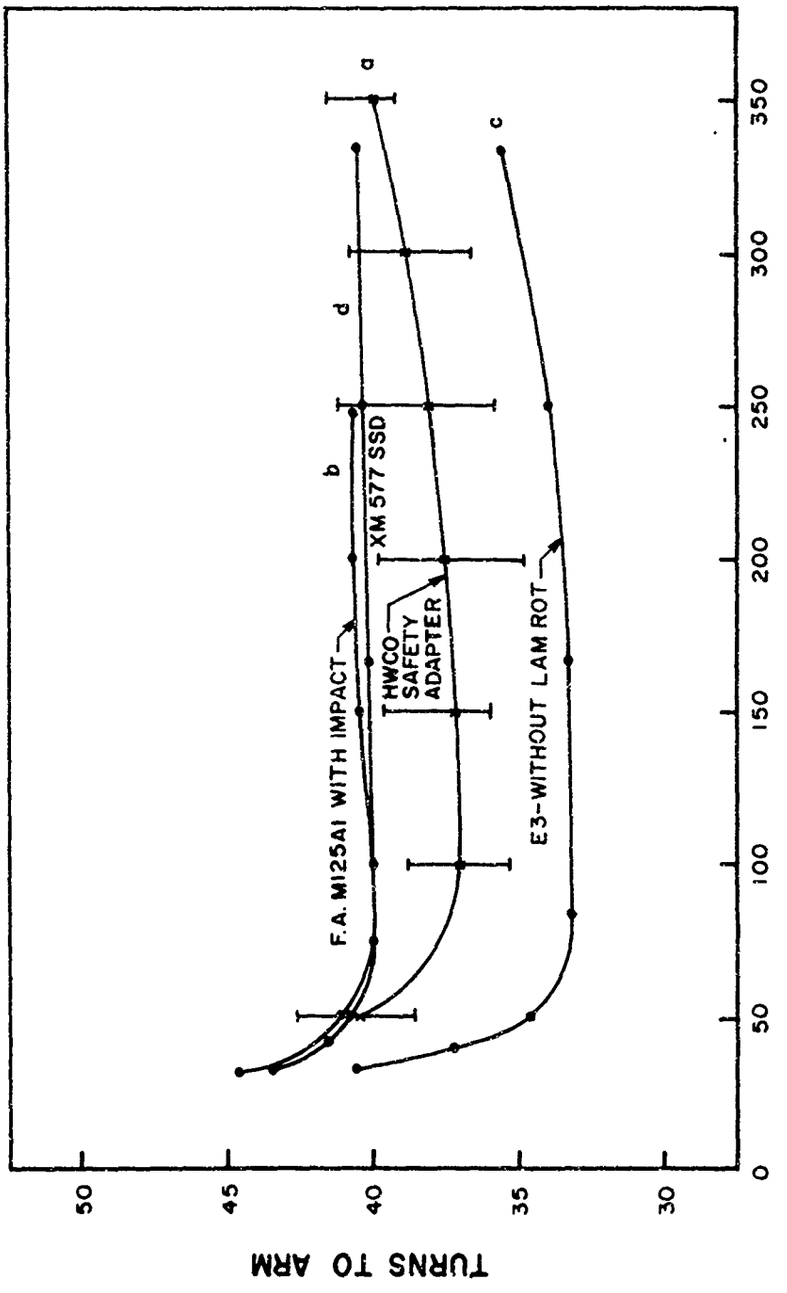

Figure 10. Experimental turns-to-arm results

To determine if the upward curvature in turns-to-arm at the higher spin speeds was a true performance characteristic and not due to experimental error, additional experiments were run under different conditions. The results are shown as curves (b), (c), and (d) on figure 10. Curve (b) represents the average data from simultaneous measurements of arming time and turns-to-arm made on nine slightly modified model A1 booster mechanisms from a different manufacturer. The test equipment was a vertical axis, direct-coupled spinner with a rotor-release fixture and timer start system that was basically different from that used in the initial Kodak spinner tests. Each unit was run under a different sequence of speeds to mask any "wearing-in" effect. Direct measurements of turns-to-arm were in precise agreement with turns-to-arm computed from the simultaneous arming-time data for this test. The fact that there was no increase for the last data point on the curve may be a chance deviation in the experimental results rather than a valid property of the mechanism. (The test fixture also vibrated badly at this last speed.)

Curve (c) is the average data from arming-time measurements made on seven M125A1E3 units (from two different manufacturers) using the same vertical axis, grinder-motor spinner and actuation system used for the tests of curve (b). The E3 mechanism is entirely different in design than the A1 having modular construction, one less stage of gearing, and an escapement with acute angle escape-wheel teeth and a pallet that spans two teeth instead of one as in the A1 design. The A1 and E3 escapements are compared in figure 11.

Curve (d) is the average data from simultaneous measurements of arming time and turns-to-arm made on five SSD modules from the XM577 mechanical time fuze. The test equipment was the same as that used to obtain curves (b) and (c). The XM577 SSD mechanism has an escapement design similar to that of the A1 booster mechanism, but there is one less gearing stage and the rotor is much less massive and rotates clockwise rather than counterclockwise when viewed from the top.

Because all four curves of the experimental data covering two different kinds of test equipment, two different test methods, three different mechanism designs, and five different manufacturers have the same tendency to upward curvature at the higher spin speeds as spin speed increases, it can only be concluded that the upward curvature is a valid performance characteristic. Thus, the present mathematical model should be refined to include this effect as discussed in section 8.2.

Some experiments were made to determine the approximate percentage of engaged motion between the pallet pin and escape-wheel tooth impulse face as discussed in section 2.5. In these tests, the escape-wheel teeth were painted with dark blue layout dye and the rotor was driven by hand at various torques. Resulting disturbances in the dye coating gave a fairly accurate indication of the impact point of the pallet pin on the impulse face of the tooth. Two M125A1 booster units from the same lot were used for the tests: one that ran fast at about 33 to 37 turns, and one that ran slow at about 43 turns.

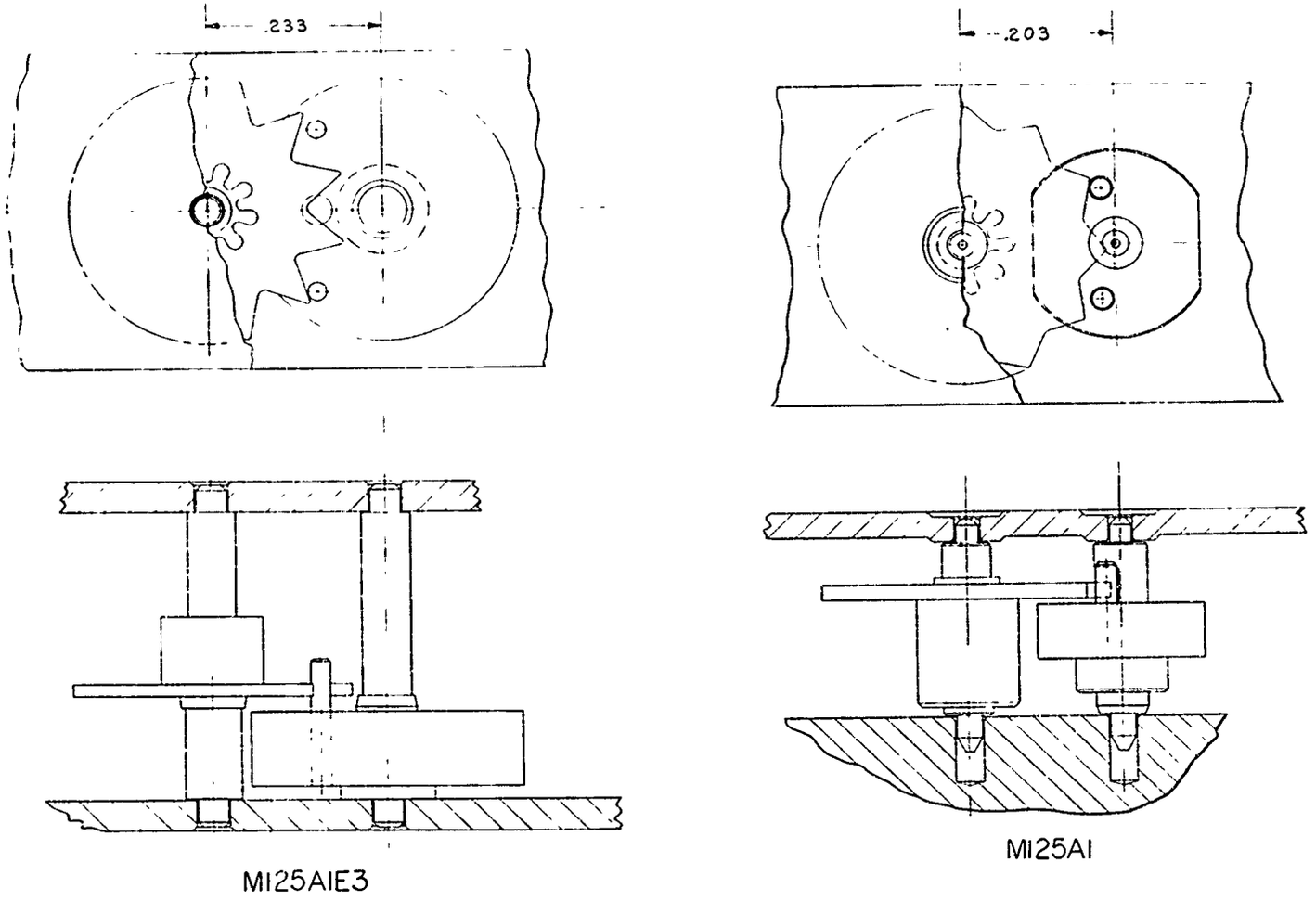

Figure 11. Comparison of the A1 and E3 runaway escapements

The percentage of engaged motion varied, depending on both the unit and the drive torque. For the fast unit, engaged motion increased from about 40 percent at a "low" drive force to the range of 45 to 50 percent for "high" drive force. For the slow unit, engaged motion increased from a 50- to 55-percent range at the low drive force to the range of about 58 to 68 percent at the high drive force. (The numerical estimates were obtained by visual judgement of the relative position of the impact point along the impulse face.) The increase in percentage of engaged motion with an increase in drive torque was an expected possibility, because of the work described by Minnix[1] on the detached lever escapement; his work shows that under higher drive torques, the escape wheel has higher acceleration and thereby "catches up" with the pallet pin sooner. However, the action of the detached lever escapement differs entirely from that of the runaway escapement; it is therefore conceivable that the percentage of engaged motion could even decrease with increased torque for certain runaway escapement designs or regions of operation.

High-speed movies at approximately 6,300 frames/sec were made of the escapement running under relatively high torque. They substantiate the observation that the percentage of engaged motion is approximately 55 percent. They also showed that the escape wheel does not noticeably recoil under impact from the pallet pin and that the pallet pin does not noticeably bounce away from the impulse face during impact.

The values obtained for percentage-engaged motion are about twice the values needed to make the present mathematical model agree reasonably with the experimental turns-to-arm data (see sect 3, 5, 6, and 7). This is not serious, however, because the mathematical model for escapement damping (see eq 24) was selected rather arbitrarily and could easily be in error by a factor of two. In fact, dividing C_E by 2 and increasing P accordingly can produce almost exact agreement between theory and experiment as discussed in section 8.2.

6. SIMPLIFIED ANALYTICAL SOLUTION

The phase I equation of motion (41) describing the operation of the booster mechanism is nonlinear in the $\dot{\theta}^2$ and sin θ terms. For this reason, it is impractical if not impossible to obtain an anlytical solution to the exact equation. However, the performance of runaway-escapement mechanisms of this type can often be described adequately by a greatly simplified form of the equation. Accuracy of the simplified solution can be checked by comparing the results with the results obtained from a computer solution of the exact equations, which is done in section 7.

---

[1] "The Development of a Mathematical Model of the Detached Lever Escapement," by Dr. Richard B. Minnix, VMI Physics Dept. under contract no. DA-49-186-AMC-176 (D) with Harry Diamond Laboratories, July 1968.

The first simplifying assumption to be made is to assume that the rotor delivers a constant drive torque under spin instead of one that varies with the sine of the rotor displacement. This is done by replacing the sin θ term by the mean value of the sine function (c) over the interval of engagement with the escapement (see eq 33).

The second simplifying assumption is to assume that the acceleration of the rotor is negligible for most of the coupled motion. Thus, the $\ddot{\theta}$ term becomes equal to zero. Although this assumption may not be too valid for the case where the driving torque varies according to a sine function, work at HDL has indicated that a runaway escapement driven by a constant driving torque accelerates to a constant running rate within 3 to 4 oscillations of the pallet. This is only about 3 percent of the coupled motion for the booster mechanism rotor, so the error involved in assuming a constant rotor velocity should be small.

The final assumption to be made is that the phase II motion (after the rotor becomes disengaged from the gear train) takes place so quickly that the time involved in this phase is negligible compared with the time required for the coupled phase of the motion. Thus, the phase I equation can be used to compute the full arming time.

With the aid of these three assumptions, equation (41) reduces to the following simplified equation describing the mechanism's performance:

$$\frac{54.85}{\eta^3}\,\dot{\theta}^2 = n^2\,(0.0964\eta^4 - \mu f) - \tau_0 . \tag{52}$$

When values for μ and η are substituted, equation (52) becomes

$$C\,\dot{\theta}^2 = n^2 D - \tau_0 , \tag{53}$$

where

$$D = 0.0964\eta^4 - \mu f , \tag{54}$$

and C is defined by equation (40), and τ_0 by equation (45). Solving for $\dot{\theta}$,

$$\dot{\theta} = \sqrt{\frac{n^2 D - \tau_0}{C}} , \tag{55}$$

which shows that the rotor speed is constant for a given spin speed (n).

Separating variables and integrating gives

$$\theta = t\sqrt{\frac{n^2 D - \tau_0}{C}} . \tag{56}$$

A given arming angle ($\Delta\theta$) occurs in a specific time (t_a), so

$$\Delta\theta = \sqrt{\frac{n^2 D - \tau_0}{C}}\; t_a . \tag{57}$$

Solving for the turns-to-arm (nt_a) gives

$$nt_a = \Delta\theta \sqrt{\frac{C}{D - \tau_0/(n^2)}} . \qquad (58)$$

Thus, the turns-to-arm is directly proportional to the rotor-arming angle and proportional to the square root of the ratio of escapement damping torque to the net driving torque. In this equation, the turns-to-arm is a function of the spin speed because of the threshold torque term τ_0 . For large values of n , the ratio n_0/n becomes insignificant and nt_a approaches a constant value of

$$nt_{a\ min} = \Delta\theta \sqrt{\frac{C}{D}} \quad . \qquad (59)$$

Substituting values in equation (58) gives,

$$nt_a = \frac{80}{57.3} \sqrt{\frac{54.85}{0.0964\eta^4 - \eta^3(\mu f + \tau_0/n^2)}} . \qquad (60)$$

For $\eta = 0.98$,

$$nt_a = 1.396 \sqrt{\frac{58.28}{0.0889 - [0.1850\ \mu + (n_0/n)^2 (0.0597 - 0.1850\mu)]}} . \qquad (61)$$

Equation (61) was used to develop the curves shown in figure 12. Curve (a) represents a set of baseline conditions. Curve (b) illustrates the effect of a lower starting friction or threshold level. Curve (c) illustrates the effect of variable pivot friction. Curve (d) illustrates the effect of changing the escapement damping action. The value of C=45 corresponds to a value of engaged motion of 16 percent instead of P=0.25 as used to compute C=58.28. Curve (e) is the experimental data of figure 10 (a). It is readily seen that the simplified theoretical equation (58) gives a very close prediction of actual performance. The escapement damping factor (C), and more exactly, the percentage engaged motion (P) and related escapement linkage ratio (N_E) as discussed in section 3.4, is the most significant variable to use for correlating theory with measured data.

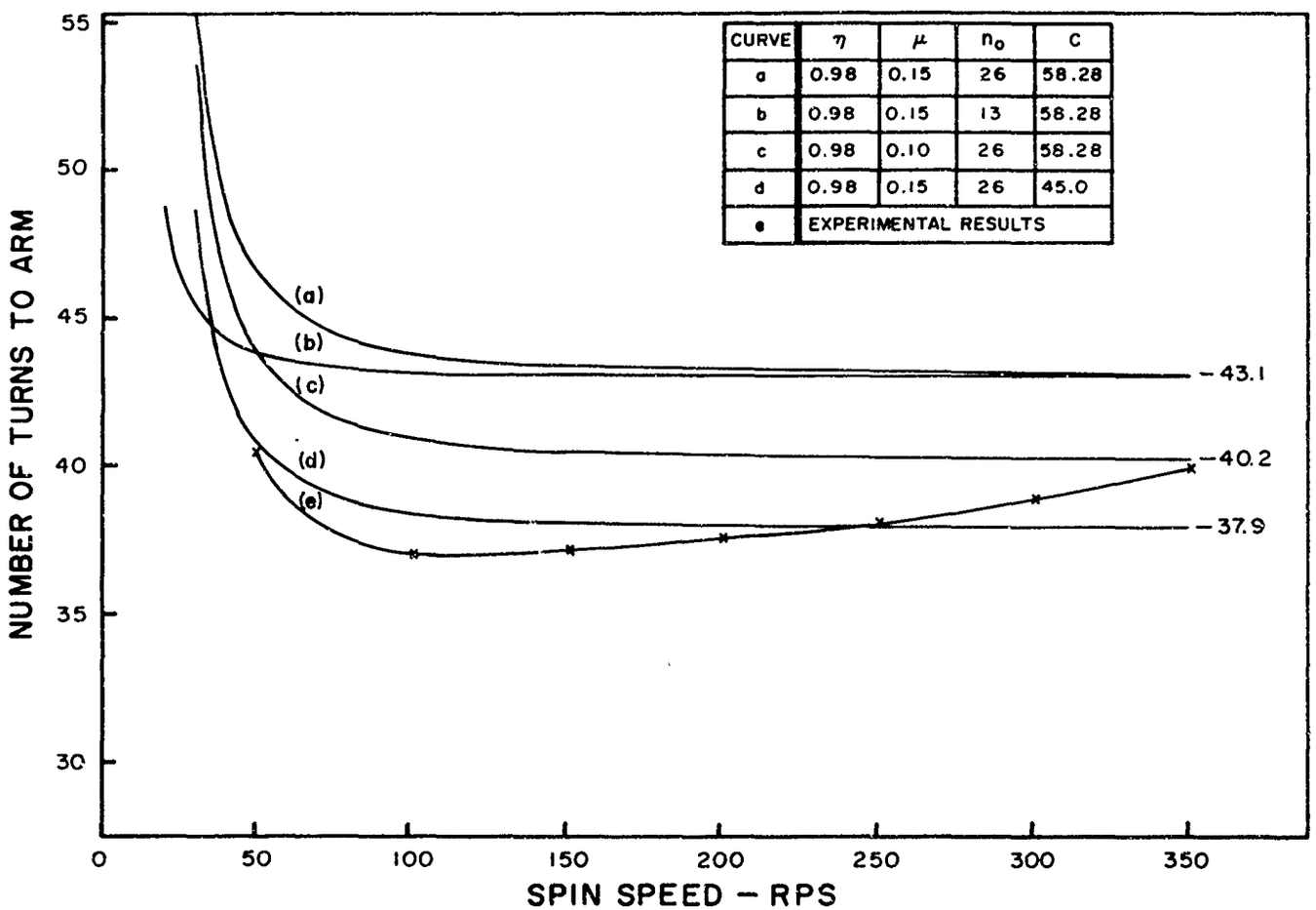

Figure 12. Results of simplified analytical solution for mechanism performance

7. COMPUTER SOLUTION

Equations (41) and (43) were set up for solution on the digital computer, using the Adams-Moulton (predictor-corrector) method of integration (see acknowlegements). The computer output for the nominal escapement parameters is shown on figures 13 through 23. Figures 13 through 15 (employing the same three methods used to present the experimental results of figures 8 through 10) show the theoretical performance over the range of spin speeds. Figure 13 shows arming time versus spin speed; the curve is generally hyperbolic in shape. Figure 14 shows arming-cycle rate or inverse time versus spin speed, and it is almost a straight line. Figure 15 which shows turns-to-arm versus spin speed gives the most descriptive picture of the mechanism performance. Comparing figure 15 with figure 12, curve (a) shows that the simplified solution developed in section 6 (eq 58) gives turns-to-arm results only about 3 percent lower than that given by the exact non-linear differential equation of motion. Another significant result is that the exact differential equations of motion developed in this analysis do not predict the upward curvature in the turns-to-arm characteristic at high spin speeds as shown by figure 10 and discussed in section 5.

The experimental results have not been overplotted on figures 13 through 15, because no detailed attempt was made to fit theoretical to experimental data. The fact that the theoretical results are about 6 or 7 turns greater than that from the experimental results is not significant because of the rough estimates that were made for the coefficient of friction at the pivots, the gear train and escapement mesh efficiencies, and the damping coefficient due to escapement action. It is the general shape of the theoretical curves that is important at this point and not their numerical values. (One attempt at close fitting of theory with experiment is discussed in section 8.2.)

One advantage of using the computer to solve the equations of motion is that it allows a detailed examination of the variation in rotor motion throughout the arming cycle. Figures 16 through 23 show the rotor's predicted displacement, velocity, and acceleration (in radian units) versus time for speeds of 30 and 100 rps (speeds representing an 11-to-1 range of rotor drive torques). These figures (16-23) are separated into two groups of four: the first four (16-19) are for 30 rps; and the second four (20-23) are for 100 rps. The first figure in each group shows the overall motion, whereas the last three in each group show a breakdown of the overall motion into three phases using expanded scales. The first phase is the acceleration (or deceleration) shown in figures 17 and 21, the second is an approximately constant running-rate phase as shown in figures 18 and 22, and the last is the free-motion phase shown in figures 19 and 23.

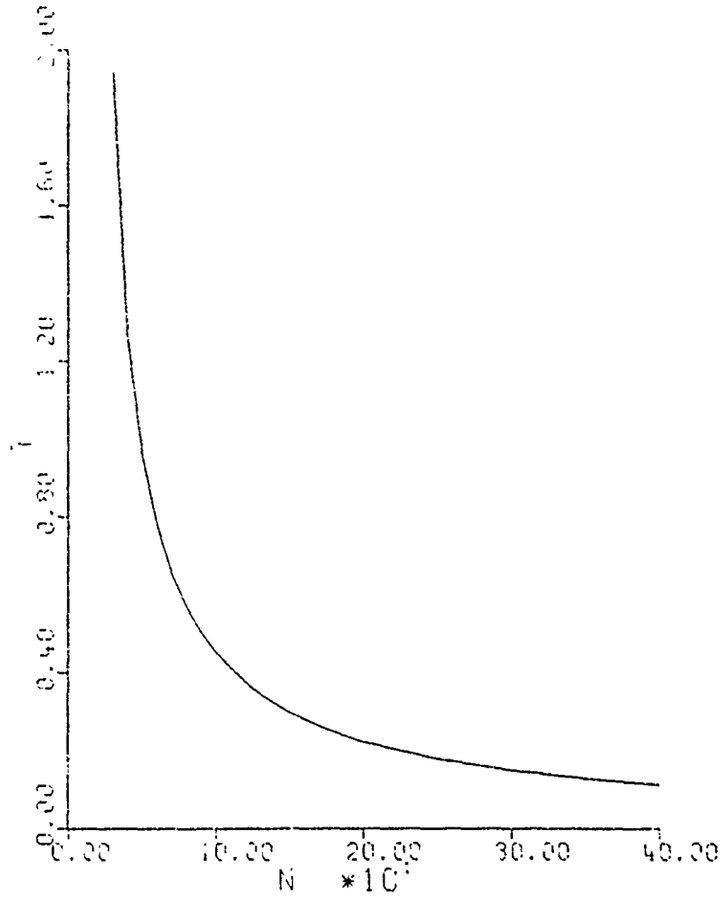

Figure 13. Theoretical arming time versus spin speed

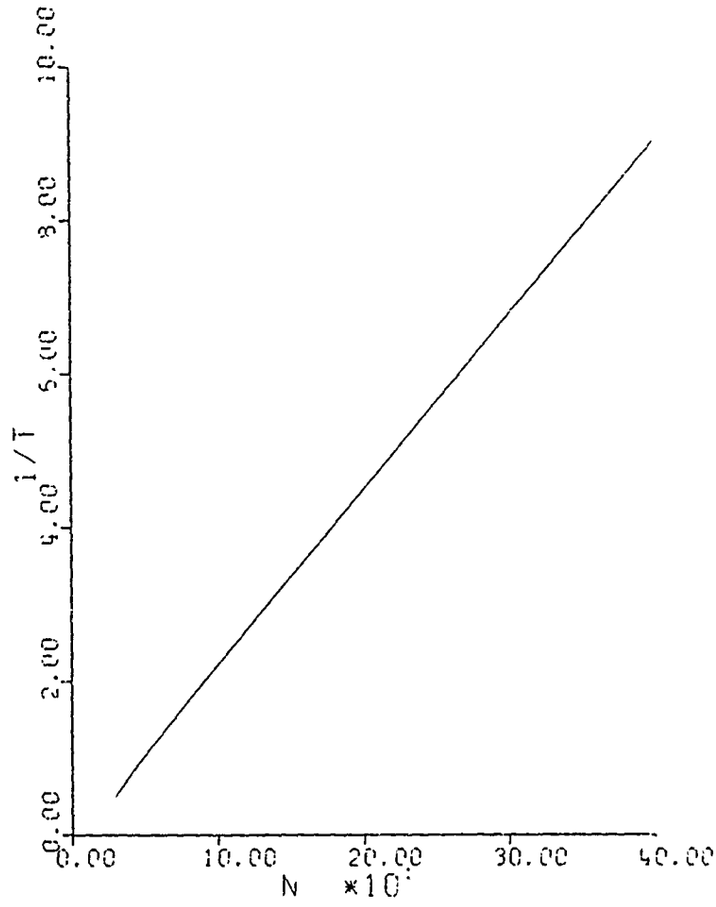

Figure 14. Theoretical arming cycle rate versus spin speed

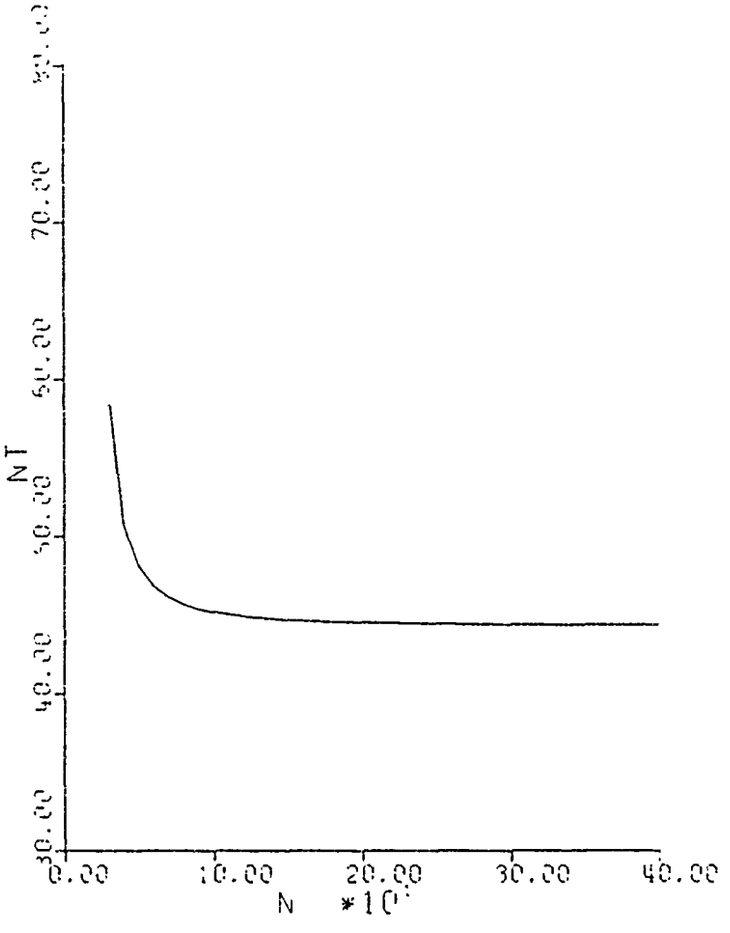

Figure 15. Theoretical turns-to-arm versus spin speed

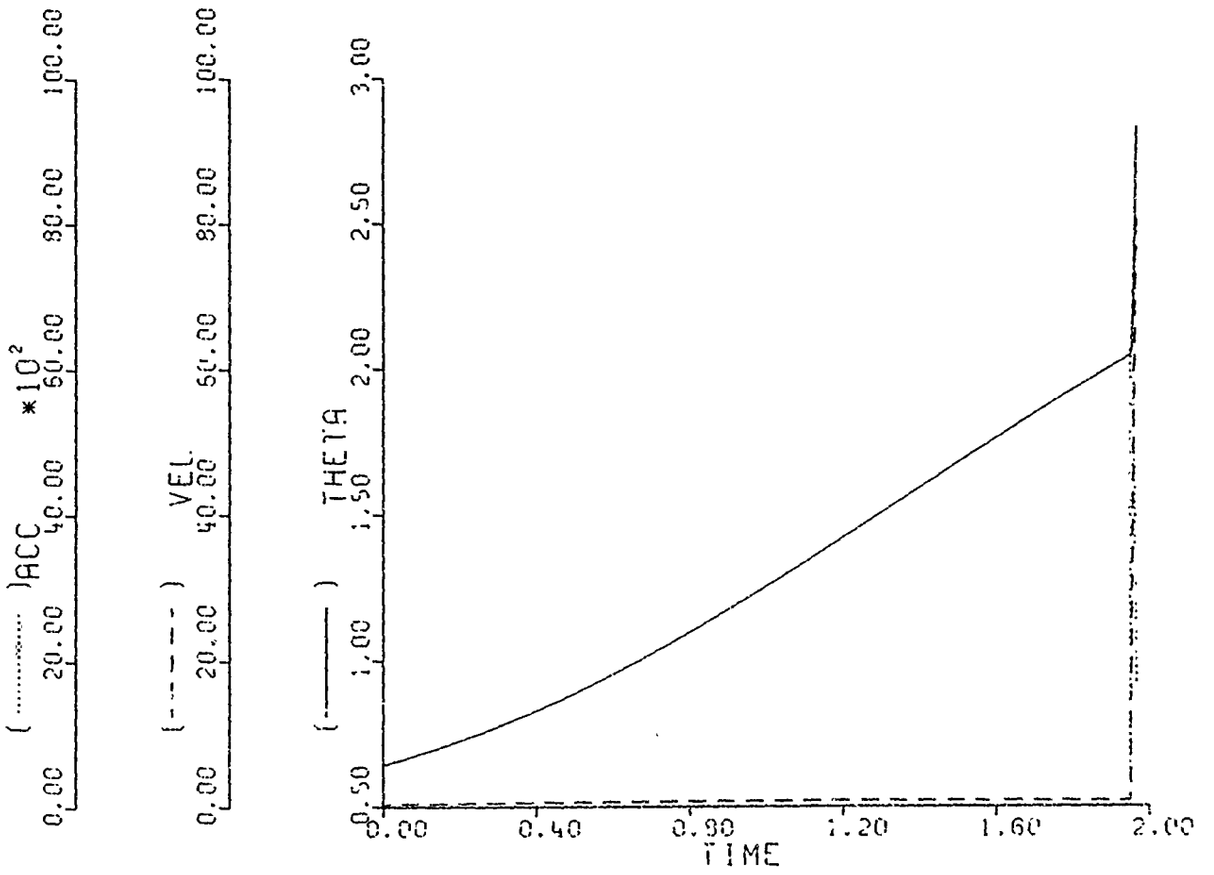

Figure 16. Rotor motion versus time at 1800 rpm

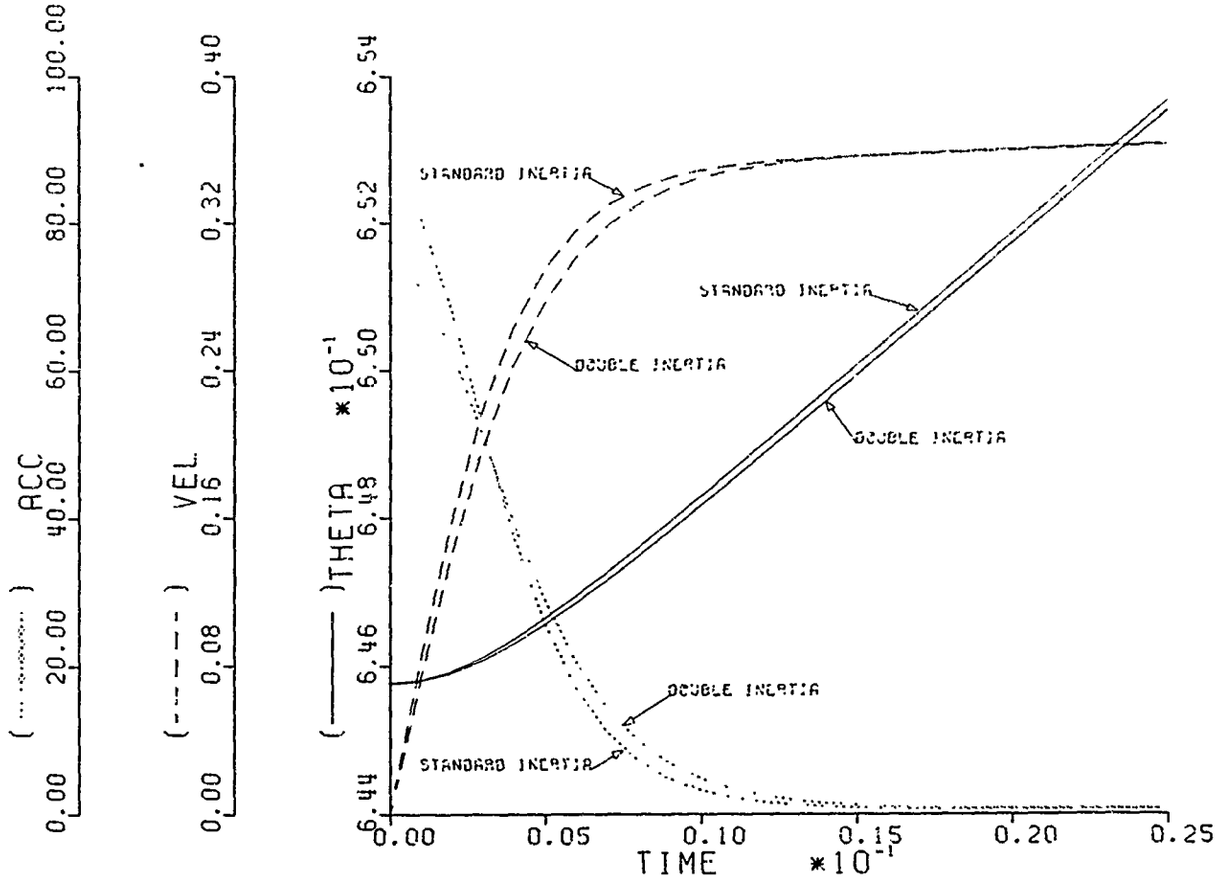

Figure 17. Acceleration phase of rotor motion N = 30

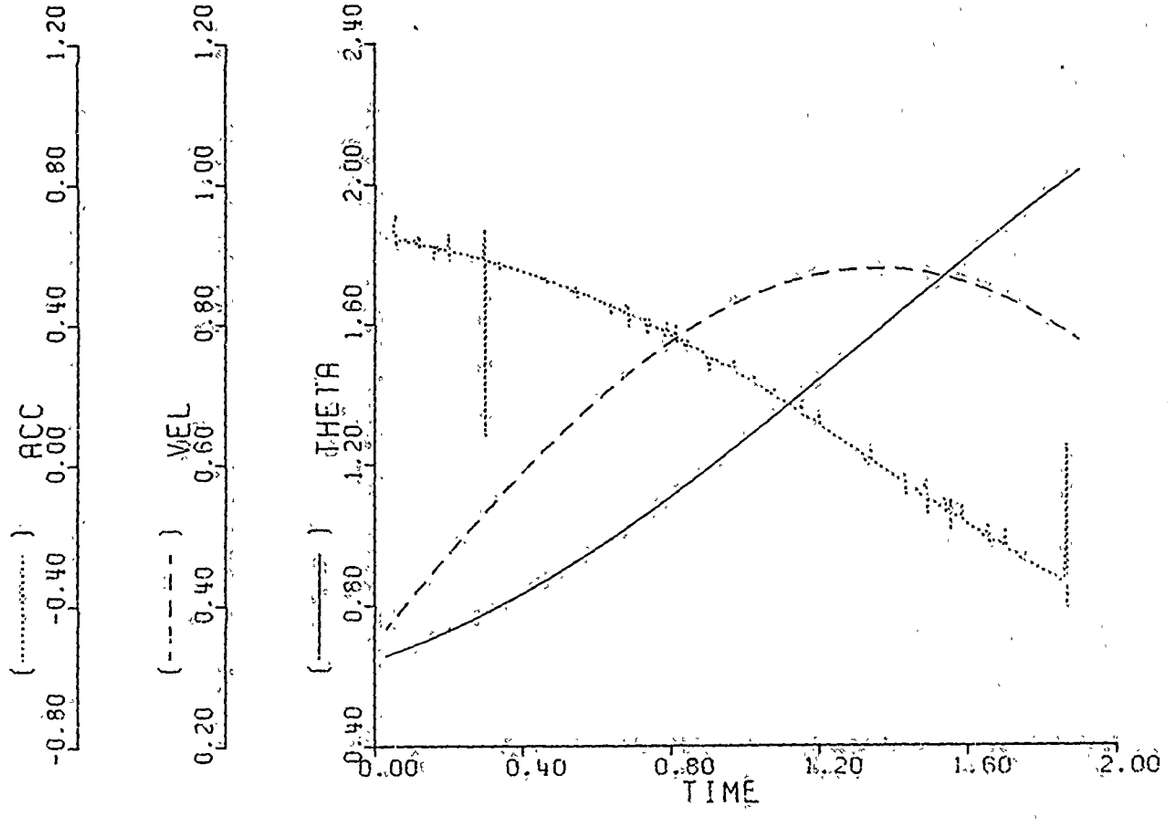

Figure 18. Delay phase of rotor motion

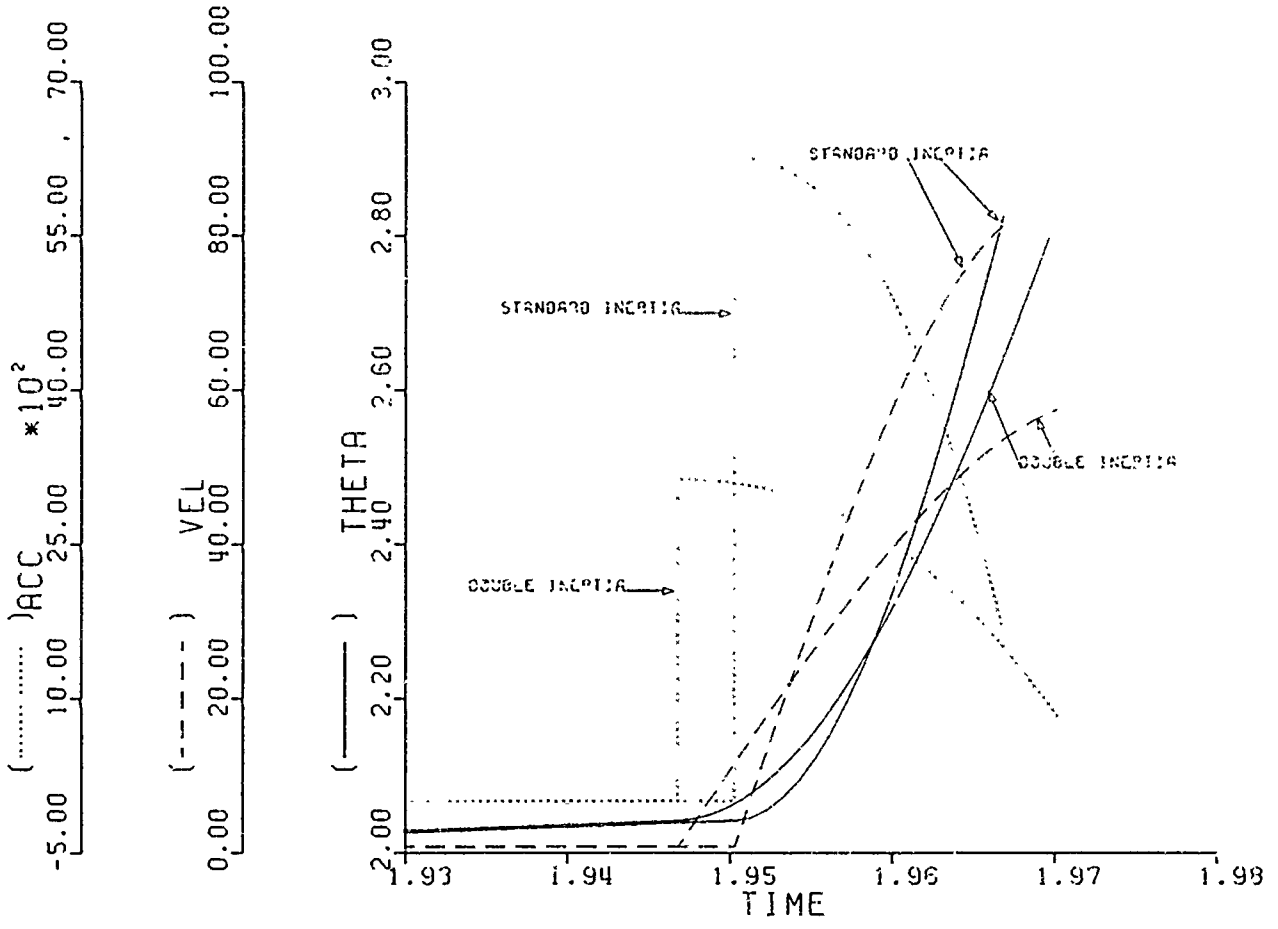

Figure 19. Free motion phase for rotor N = 30

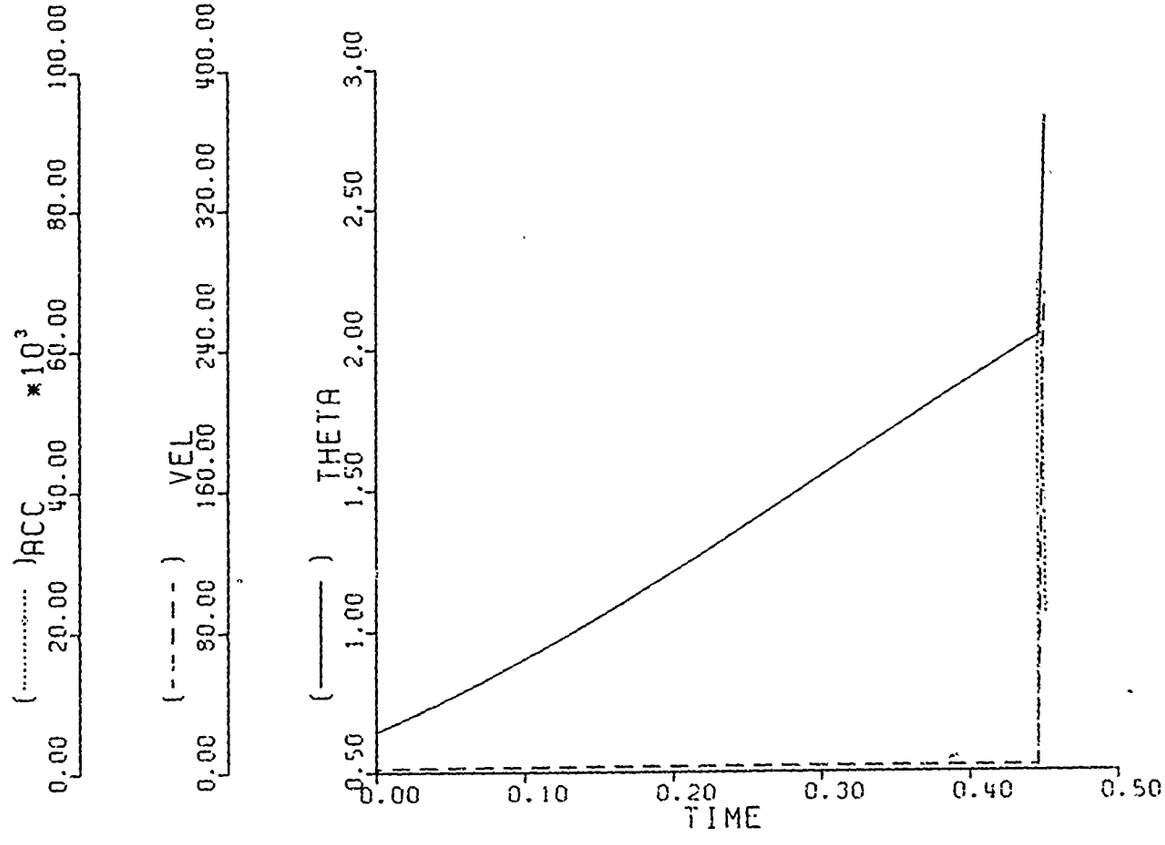

Figure 20. Rotor motion versus time at 6000 rpm N = 100

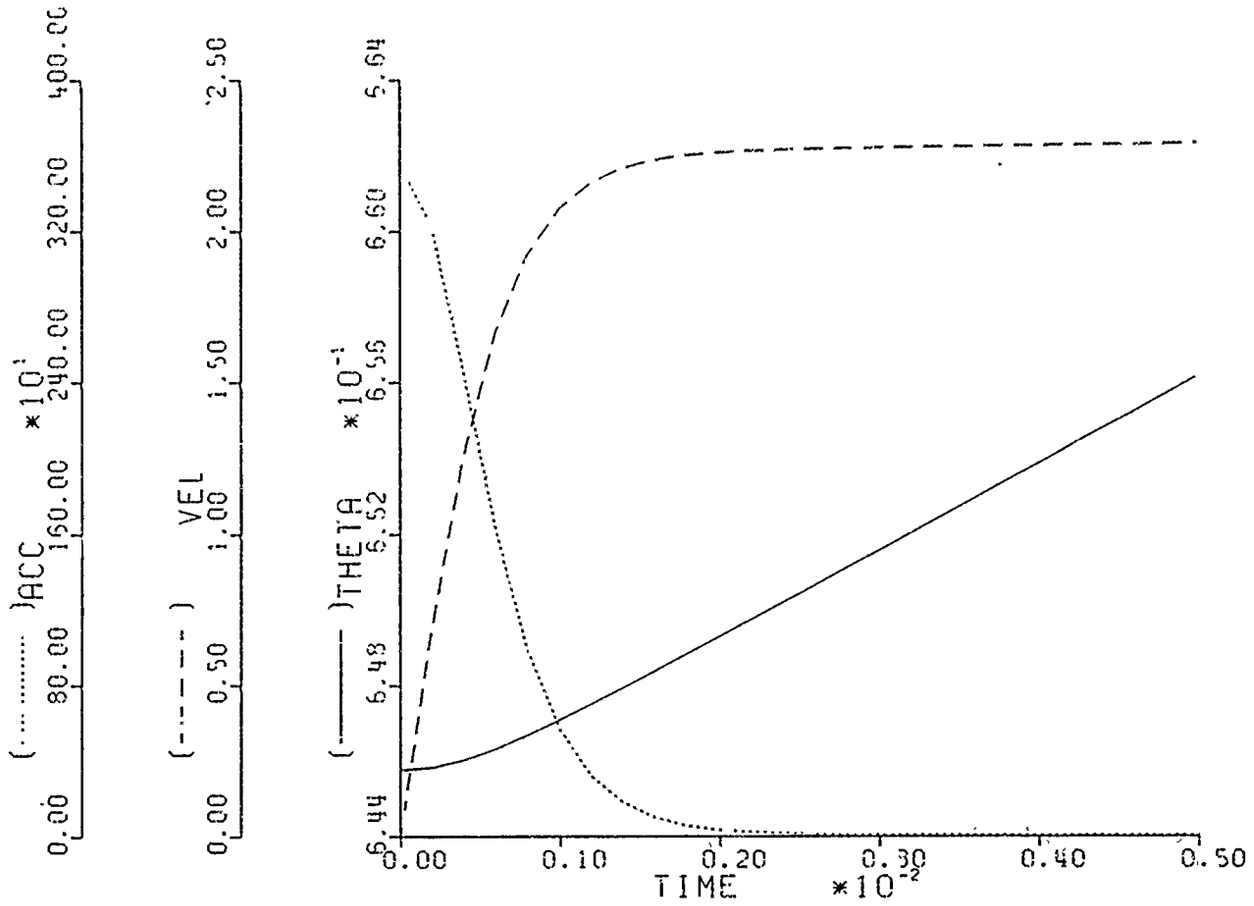

Figure 21. Acceleration phase of rotor motion N = 100

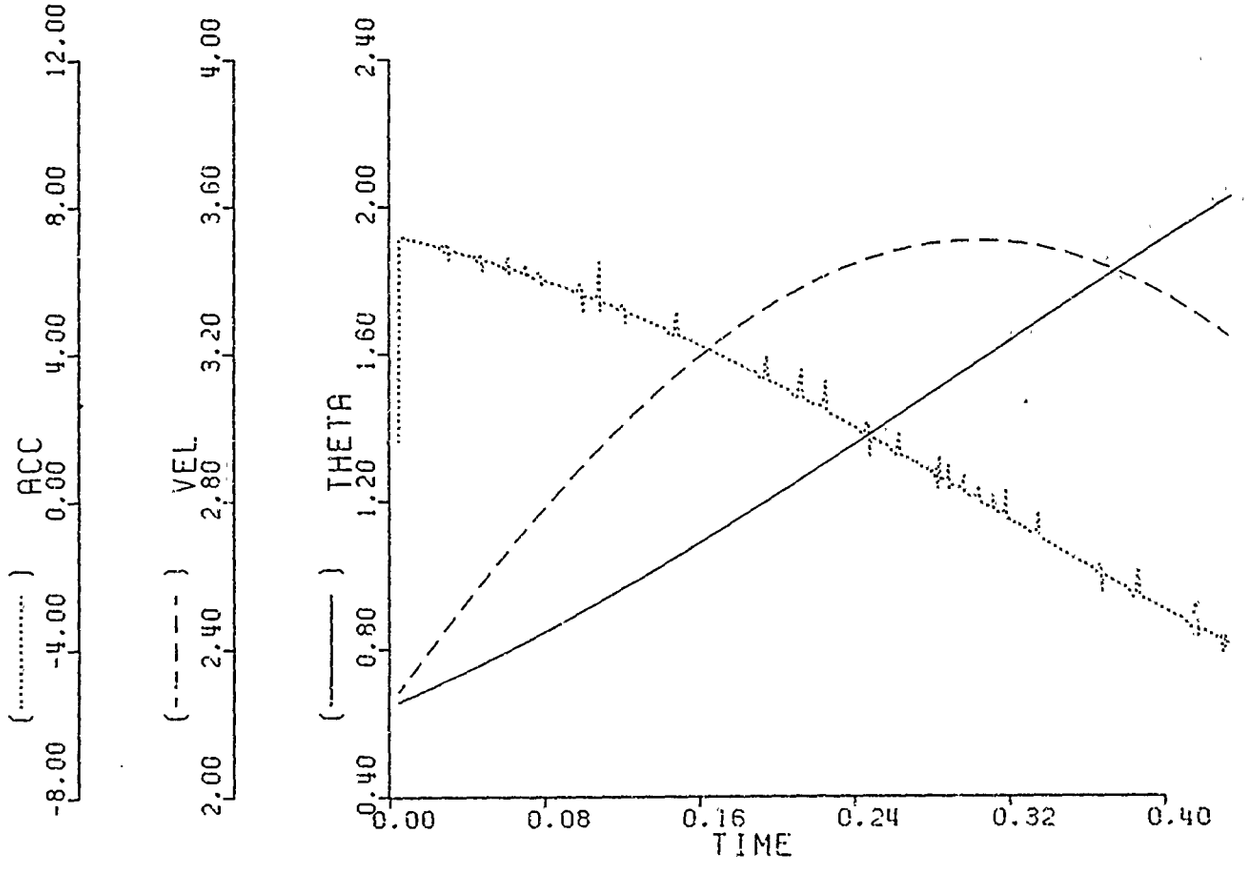

Figure 22. Delay phase of rotor motion

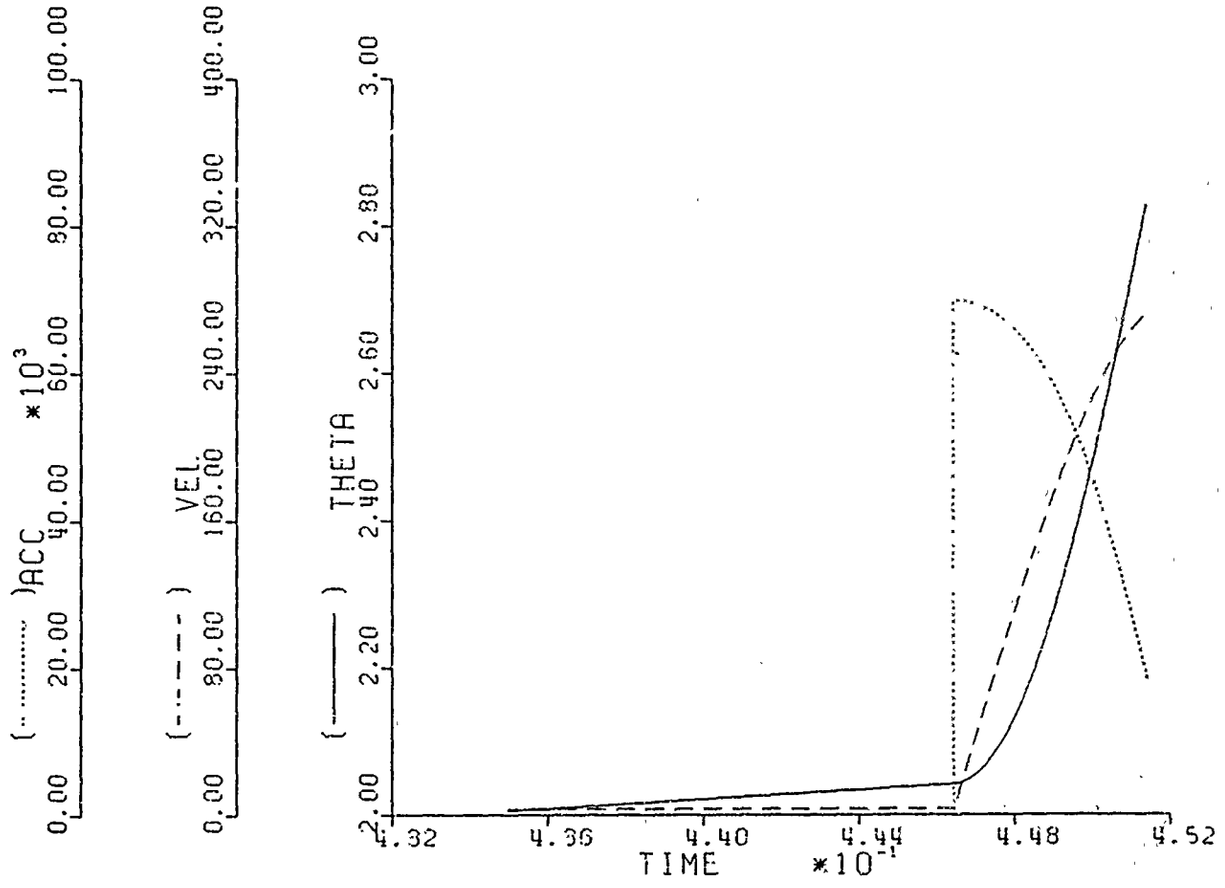

Figure 23. Free motion phase for rotor

A study of these eight figures reveals the following:

(a) The time required for the acceleration and free-motion phases combined is negligible when compared with the overall arming times (about 1.5 and 1.8 percent of the total arming times of 1.97 and 0.45 sec for N=30 and N=100 rps, respectively).

(b) The acceleration phase takes place faster as the spin speed increases, and the 45 deg of free motion takes place in about 16 msec for N=30 rps and 5 msec for N=100 rps.

(c) Using figures 16 and 20, the rotor appears to move at essentially constant velocity (zero acceleration) while engaged with the gear train, but this is not the case. Examining figures 18 and 22, the effect of the sine function in the driving torque term becomes apparent. It causes the acceleration term to have finite values and to pass through zero and go negative as θ reaches exactly 90 deg. The large excursions ("hash") on the nominal acceleration curves in figures 18 and 22 are the result of the computer solution method only and are caused by the fact that the acceleration values do not come from an integration process. (Double precision was used during these calculations.) The rotor velocity also follows a sinusoidal characteristic and has a peak value at exactly 90-deg displacement.

(d) In figures 19 and 23, the rotor acceleration changes instantaneously as the rotor drops off the gear train and is no longer influenced by the escapement damping torque. The acceleration then falls off according to the driving torque sine function as θ goes from 117 and 162 deg and the rotor velocity increases to a peak value (2600 rpm for N=100 rps) at the instant the rotor impacts the rotor stop.

One of the motivating factors for this theoretical analysis was a debate about whether or not the rotor's inertia had a large influence on the turns-to-arm performance of the booster mechanism. To evaluate this factor, the rotor inertia was artifically doubled, keeping all other design parameters the same, and the computer program (represented by fig. 13 through 23) was rerun. Little effect was expected because the acceleration and free-motion phases account for such a small portion of the overall arming time, the gear train accounts for over 85 percent of the effective rotor inertia for the standard case, and the effect of the increased rotor inertia on escapement damping action (see equations 18 and 24) is very slight. (The value of $C_\eta{}^3$ from equation 40 decreases from 54.85 to 54.62, as I_ϕ increases from 37.5 to 43.0 X 10^{-6} gm-cm-sec^2.)

Some results of the double inertia computer run are illustrated in figures 17 and 19 for a spin speed of 30 rps. As expected, the acceleration and free-motion phases take slightly longer, but the mechanism runs only slightly slower overall (3 msec or 0.15 percent) when the rotor inertia is doubled. The relative effect of double rotor inertia at 100 rps was essentially the same as that obtained at 30 rps; thus, only the 30-rps results are given. The effect of double rotor

inertia on turns-to-arm was to increase this parameter by only 0.12 turns or about 0.3 percent. Because the effect is so slight, it is not shown on figure 15, but the curve would run essentially parallel to and about 0.012 in. above the theoretical turns-to-arm curve for the standard inertia rotor.

The effect of variations in other design parameters such as rotor excursion angle, rotor mass, rotor center of gravity location, gear-train friction, pallet inertia, percent engaged motion, and changes in escapement geometry as reflected in the linkage ratio are most easily determined, using equation (59) and all ancillary equations. Keep in mind that the results of equation (59) differed by only 3 to 4 percent from the results of equations (41) and (43). Thus, variations in rotor excursion affect turns-to-arm directly; variations in escapement design parameters affect turns-to-arm directly through the square root of the overall damping coefficient; and variations in rotor mass, center of gravity location, and pivot friction affect turns-to-arm inversely as the square root of the net drive torque term. It is seen that the effective rotor-arming angle during engagement with the escapement is the most significant variable affecting performance. Note that this variable includes backlash in the gear train and rotor-release mechanism and probably accounts for much of the difference between curves (a) and (b) of figure 10.

8. SUMMARY

8.1 Conclusions

Specific conclusions that can be drawn from the work covered by this report follow.

(a) The rotor drive torque at a given spin speed can be expressed as a function of a single variable ($\sin \theta$) as shown by figure 3 and equation (6).

(b) The equations for the escape-wheel velocity versus the amount of engaged motion as developed by Hausner and VMI[1] can be combined into a single expression (24) and used to compute a relatively accurate value of the damping coefficient for the M125A1 escapement mechanism.

(c) The damping coefficient is highly dependent on the percentage of engaged motion and corresponding average linkage ratio for the escapement as indicated by figure 6.

(d) The turns-to-arm performance of the mechanism can be predicted fairly accurately, using the equations developed in sections 2 and 6.

---

[1] "A Study of the Dynamics of an Untuned Clock Mechanism," VMI Dept. of Physics, Lexington, Virginia; under contract CST-1224 (DAI-49-186-ORD (P)-100) with Harry Diamond Labs, 1 Sept 1953.

(e) The analytical solution (eq 58 and fig. 12) of the simplified equations of motion gave results within 3 percent of the results produced by computer solution of the detailed equations of motion (26) through (30) and figure 15. Thus, the assumptions of mean value for the rotor-drive torque, and negligible time required for the acceleration and free-motion phases of the operation yield good results.

(f) There is an upward curvature in the turns-to-arm characteristic at the higher spin speeds and the present equations of motion do not predict it (see fig. 10, 12, and 15). Thus, the escapement-damping action is not only a function of the square of the rotor velocity and a constant coefficient; it is also dependent on the rotor or escape-wheel drive torque.

(g) The turns-to-arm characteristic is the most sensitive and most meaningful parameter for expressing the performance of a given design or a given device.

(h) The effect of rotor-inertia variations on the turns-to-arm performance is negligible.

(i) During operation, the pallet pins engage the escape-wheel tooth impulse face over only approximately half of its length.

8.2 Discussion

The analysis presented to this point has treated damping-torque variations as a function of the ratio of free-to-engaged motion (P) or the corresponding average escapement linkage ratio (N_E) for the escapement action. By assuming a constant value for this parameter, it was shown that an overall damping coefficient could be calculated (eq 40) that would give reasonable agreement between theory and experiment. However, it was noted that the analysis did not predict the distinctive upward curvature in the experimental turns-to-arm characteristic (see 8.1, f).

There are many possible ways of modifying the analysis to induce the rising trend in the turns-to-arm curve. Although it was not intended to conduct such a detailed analysis in this report, one very simple method is suggested by the experimental result of the pallet-pin impact point along the escape-wheel tooth impulse face. A brief explanation of a modified analysis using this method is given to illustrate how the mathematical model can be refined to obtain much closer agreement between theory and experiment.

In order to cause turns-to-arm to increase with spin speed in equation (58), the damping coefficient (C) is made to be a function of the spin speed by including a variable engagement factor ($\Delta P/\Delta n$) in equation (24). (This equation is also arbitrarily divided by a factor of 2 to allow P_0 to be closer to the experimental value.) $\Delta P/\Delta n$ will be positive so that engagement increases with spin speed. The resulting mathematical model is summarized in figure 24. The analytical results obtained from this model with initial engagements

Figure 24. Summary of a refined analytical model of the M125 booster mechanism

(a) $$N = nt_a = (\theta_1 - \theta_0)\sqrt{\frac{C_\eta}{D - \tau_0/(n^2)}}$$

(b) $$C_n = \frac{C_E\,(N_1 N_2 N_3)^3}{\eta^3}$$

(c) $$C_E = \frac{N_E^2 I_p\,(I_e + PN_E^2 I_p)^2}{\psi I_e\,(I_e + N_e^2 I_p)}$$

(d) $$N_E = N_T - \left(\frac{N_T - N_R}{2}\right) P$$

(e) $$P = P_0 + (\Delta P/\Delta n)\,(n - n_0)$$

(f) $$D = \frac{arm_R \eta^4}{\theta_1 - \theta_0} \int_{\theta_0}^{\theta_1} \sin\theta\, d\theta - \mu f$$

(g) $$f = m_R r r_{pR} + \frac{N_1}{\eta} m_1 r_1 r_{p_1} + \frac{N_1 N_2}{\eta^2} m_2 r_2 r_{p_2} + \frac{N_1 N_2 N_3}{\eta^3} m_E r_E r_{pE} + \frac{N_1 N_2 N_3 P N_E}{\eta^5} m_p r_p r_{pp}$$

(h) $$\tau_0 = n_0^2 (arm_R\, \eta^4 \sin\theta_0 - \mu f_0)$$

(i) $$f_0 = f(P_0, N_{E_0})$$

(j) $$N_{E_0} = N_T - \left(\frac{N_T - N_R}{2}\right) P_0$$

(k) $$I_e = I_E + \frac{I_2}{N_3^2} + \frac{I_1}{(N_3 N_2)^2} + \frac{I_R}{(N_3 N_2 N_1)^2}$$

Figure 24. (continued)

N	=	Turns-to-arm
C_n	=	Variable damping coefficient at rotor
C_E	=	Escapement damping coefficient
N_E	=	Escapement-linkage ratio
P	=	Percent engaged motion for escapement
D	=	Mean drive torque at rotor
f	=	Friction torque term
τ_0	=	Starting torque term
f_0	=	Initial value of f
N_{E_0}	=	Initial value of N_E
I_e	=	Effective escape-wheel inertia
$\Delta p/\Delta n$	=	Rate of change of engaged motion
I	=	Component inertia
a	=	Distance from rotor pivot to CG
n	=	Spin speed
η	=	Gear-mesh efficiency
P_0	=	Initial value of P
θ	=	Rotor displacement
I_p	=	Pallet inertia
ψ	=	180 deg ÷ no. of escape-wheel teeth
$N_{1,2,3}$	=	Gear-mesh ratios
μ	=	Coefficient of friction
N_T	=	Value of N_E at tooth tip
N_R	=	Value of N_E at tooth root
m	=	Component mass
r	=	Component eccentricity
r_p	=	Pivot radius
n_0	=	Minimum spin speed

(P_0) of 55 percent (with $\mu = 0.15$), 50 percent (with $\mu = 0.12$), and $\Delta P/\Delta n = 0.0005$ (5 percent increase in the engagement per 100 rps) are shown on figure 25. For these calculations, it was assumed that the value of PN_E in the fifth term of equation (g) in figure 24 remained constant at its initial value of $P_0 N_{E_0}$, so that D and τ_0 (eq f and h) remained constant. Note the improved agreement between theory and experiment not only with respect to the degree of engaged motion but in the relative slope of the curves. Obviously, the model is still far from perfect but the results indicate that futher refinement could produce essentially perfect agreement between theory and experiment.

8.3 Recommendations

It is felt that the simplified mathematical model summarized in figure 24 will be adequate for essentially any booster mechanism analysis desired. It is of simple algebraic form and describes the interrelationship between almost every parameter of interest in the mechanism. ($\Delta P/\Delta n$ can be taken positive, negative, or zero.) Any further refinement of the model should be directed toward the solution of important problems that cannot be answered accurately enough using the present form.

The main potential area for refinement would be in the damping action of the escapement. A valuable addition would be a mathematical model to determine the effective linkage ratio of the escapement to replace the present graphical procedure. It should take into account finite diameter pallet pins, rounded escape-wheel teeth, and tolerance variations on center distance, pallet-pin location, and escape-wheel geometry. A detailed dynamic analysis of the escapement action using computer solution of the VMI equations of motion and including partially elastic collisions may also prove valuable. (Note that some work has recently been done in this area.[1, 2]) Characteristic plots of the free-to-engaged motion ratio versus driving torque could be obtained, and the data could be fitted with a simple expression that could be used in combination with the linkage ratio model to refine the overall analysis.

Another area where additional work should be done is to apply the present model to other escapement designs such as the E3 and the verge pallet E4. If accurate performance predictions could not be obtained for these quite different escapement designs, the need for further refinement of the model would be clearly indicated.

Three other areas that might be considered for analysis are the possibility of a torque or speed dependent gear-mesh efficiency, mechanism operation under eccentric spin conditions, and analytical consideration of the four ballistic factors listed at the end of section 4.

---

[1] "A General Study Of Verge Escapement Performance," by Dr. J. N. Shinkle; Sandia Laboratories Report SC-RR-69-495, October 1969.

[2] "Runaway (Verge) Escapement Analysis And Guide For Designing Fuze Escapements," by M.E. Anderson and S.L. Redmond; Naval Weapons Center Report NWCCL-TP-860, December 1969.

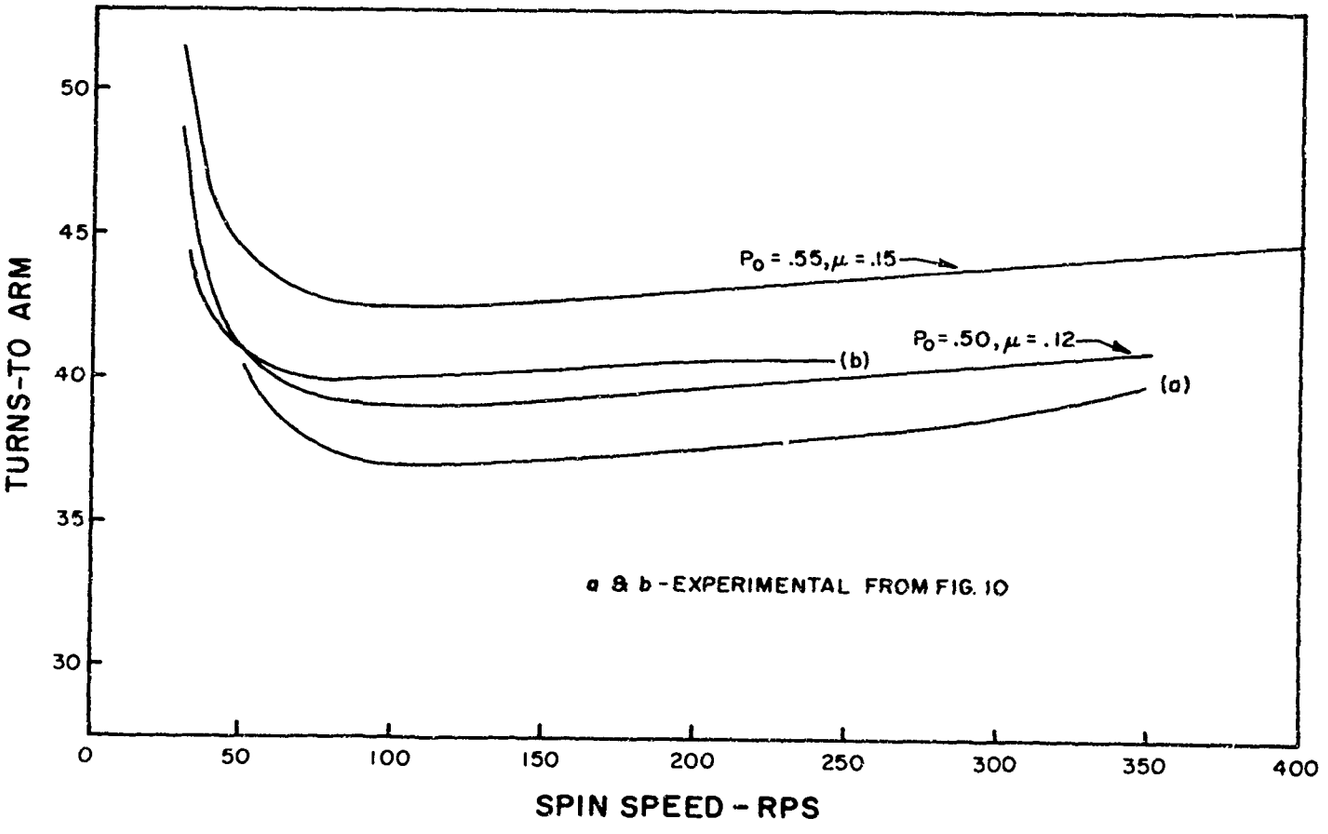

Figure 25. Results of a refined analysis of the M125A1 booster mechanism

9. LITERATURE CITED

1. "A Study of the Dynamics of an Untuned Clock Mechanism," VMI Dept. of Physics, Lexington, Virginia; under contract CST-1224 (DAI-49-186-ORD (P)-100) with Harry Diamond Laboratories, 1 September 1953.

2. "The Development of a Mathematical Model of the Detached Lever Escapement," by Dr. Richard B. Minnix, VMI Physics Dept. under contract no. DA-49-186-AMC-176 (D) with Harry Diamond Laboratories, July 1968.

3. "A General Study of Verge Escapement Performance," by Dr. J. N. Shinkle; Sandia Laboratories Report SC-RR-69-495, October 1969.

4. "Runaway (Verge) Escapement Analysis and Guide for Designing Fuze Escapements," by M. E. Anderson and S. L. Redmond; Naval Weapons Center Report NMCCL-TP-860, December 1969.

10. ACKNOWLEDGMENT

The author gratefully acknowledges the contributions made by HDL staff members C. M. Furlani, who programmed the equations of motion for computer solution and graphical presentation of the results, and I. F. Rosenkrantz and G. S. Thompson who designed test fixtures and conducted spin tests on the mechanisms; also, T. J. Krupa of Delaware Valley Armaments, Inc. who made measurements of various mechanism parameters.

GLOSSARY

Symbols and definitions			Parameter Values
a	-	distance from rotor axis to rotor center of gravity (in.).	0.0941
B	-	bore diameter of weapon.	
c	-	mean value of sin θ between θo and θ_1.	0.8972
C	-	coefficient of damping at the rotor provided by escapement action.	
C_E	-	coefficient of damping at the escape-wheel provided by escapement action.	
d	-	projectile displacement beyond muzzle of weapon.	
D	-	net rotor drive torque ignoring starting torque.	
f	-	friction term proportional to the overall torque lost due to pivot friction.	
F	-	centrifugal force	
I_1	-	inertia of 1st gear/pinion assembly (gm-cm-sec^2)	130×10^{-6}
I_2	-	inertia of 2nd gear/pinion assembly (gm-cm-sec^2)	31×10^{-6}
I_E	-	inertia of escape-wheel/ pinion assembly (gm-cm-sec^2)	27×10^{-6}
I_p	-	inertia of pallet assembly (gm-cm-sec^2)	26×10^{-6}
I_R	-	inertia of rotor assembly (gm-cm-sec^2)	0.0122
I_{Re}	-	effective inertia of rotor including gear train and escapement (gm-cm-sec^2)	0.0838

GLOSSARY Continued

Symbols and definitions			Parameter Values
I_e	-	effective inertia of escape-wheel including gear train and rotor	38×10^{-6}
m_1	-	mass of 1st gear/pinion assembly (weight-gm)	1.18
m_2	--	mass of 2nd gear/pinion assembly (weight-gm)	0.50
m_E	-	mass of escape-wheel/pinion assembly (weight-gm)	0.43
m_p	-	mass of pallet assembly (weight-gm)	0.62
m_R	-	mass of rotor assembly (weight-gm)	19
n	-	spin speed in revolutions per second	
n_0	-	spin speed required for threshold of motion (rps)	*26
N	-	proportionality constant equal to the number of turns-to-arm for the mechanism	
N_1	-	gear ratio for the rotor mesh	5.25:1
N_2	-	gear ratio for the 2nd mesh	3:1
N_3	-	gear ratio for the 3rd mesh	3:1
N_E	-	average linkage ratio for the escapement	
N_R	-	average linkage ratio at the root of an escape-wheel tooth	1.05:1
N_T	-	average linkage ratio at the tip of an escape-wheel tooth	1.98:1
P	-	percentage (time or distance) of engaged motion of the escapement action	
r	-	distance from the center of spin to the rotor axis (in.)	0.225

GLOSSARY Continued

Symbols and definitions			Parameter Values
r_1	-	distance from the center of spin to the 1st gear assy. axis (in.)	0.436
r_2	-	distance from the center of spin to the 2nd gear assy. axis (in.)	0.505
r_E	-	distance from the center of spin to the escape-wheel assy. axis (in.)	0.520
r_p	-	distance from the center of spin to the pallet assy. axis (in.)	0.433
r_{p_1}	-	first gear assy pivot radius (in.)	0.0248
r_{p_2}	-	second gear assy pivot radius (in.)	0.0181
r_{pE}	-	escape-wheel assy pivot radius (in.)	0.0165
r_{pp}	-	pallet assy pivot radius (in.)	0.0165
r_{pR}	-	rotor assy pivot radius (in.)	0.0650
R	-	overall external resistance to rotor motion	
R_E	-	resistance to rotor motion due to escapement action	
$R_{E'}$	-	resistance to escape-wheel motion caused by escapement action	
R_F	-	resistance to rotor motion caused by friction	
R_I	-	inertial resistance due to gear train and escape-wheel	
t_a	-	time required for rotor arming	
T	-	inverse twist of rifled weapon in calibers per turn	

GLOSSARY Continued

Symbols and definitions			Parameter Values
V	-	muzzle velocity of projectile	
x	-	generalized displacement coordinate	
$\eta_1, \eta_2, \eta_3, \eta_E$	-	efficiencies of meshing action for gear train and escapement	*0.98
$\theta, \dot{\theta}, \ddot{\theta}$	-	angular displacement, velocity, and acceleration of the rotor with respect to the housing	
θ_0	-	initial displacement of the rotor	37 deg
θ_1	-	rotor displacement at point of disengagement from the gear train	117 deg
θ_2	-	maximum rotor displacement (armed position)	162 deg
$\bar{\dot{\phi}}$	-	average angular velocity of the escape wheel	
τ	-	gross rotor drive torque	
τ_E	-	drive torque at the escape wheel	
τ_0	-	starting torque (equivalent to minimum operating speed)	
μ	-	coefficient of friction	*0.15
ω	-	angular velocity of projectile (rad/sec)	
ω_0	-	projectile angular velocity required for threshold of motion	
ψ	-	one-half the angle subtended by an escape-wheel tooth (ψ = 180 deg/ number of teeth)	15 deg

*The basic value selected for the analysis